AD-A083 702 JAYCOR ALEXANDRIA VA F/G 20/8
AXIAL AND RADIAL COMPRESSION OF ION BEAMS.(U)
MAR 80 S A GOLDSTEIN, P F OTTINGER N00173-79-C-0420
UNCLASSIFIED JAYCOR-TP0200-80-003-FR NL

1 OF 2
AD A083702

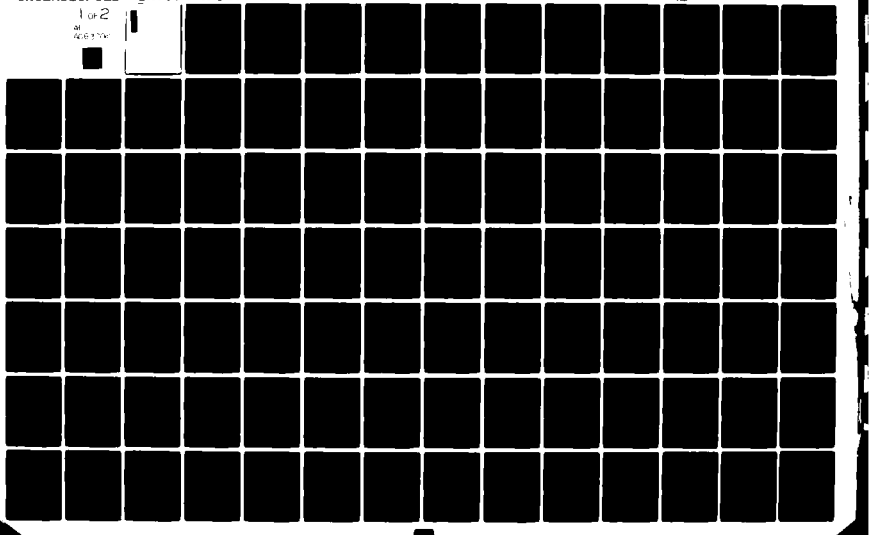

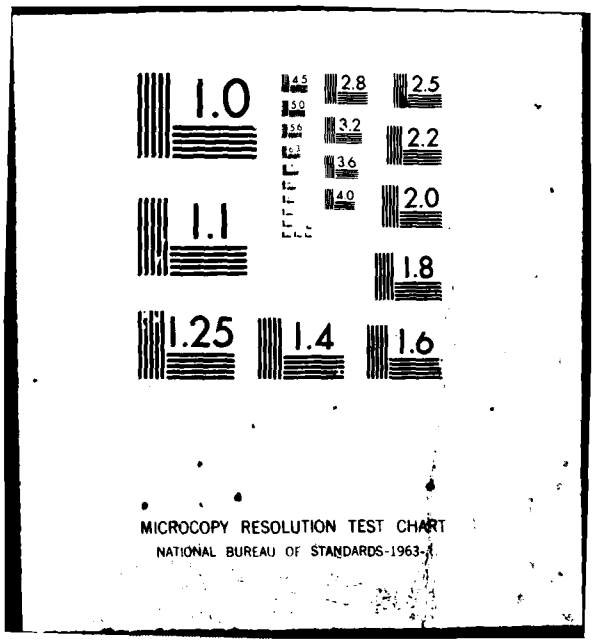
1.0
1.1
1.25
1.4
1.6
1.8
2.0
2.2
2.5
2.8
3.2
3.6
4.0
4.5
5.0
5.6
6.3
MICROCOPY RESOLUTION TEST CHART
NATIONAL BUREAU OF STANDARDS-1963-A

12

FINAL REPORT ON

AXIAL AND RADIAL COMPRESSION OF

ION BEAMS

JAYCOR Project 6144
Contract No. N00173-79-C-0420
Report No. TPD200-80-003-FR

March 1980

Shyke A. Goldstein
Paul F. Ottinger

JAYCOR
205 S. Whiting Street
Alexandria, VA. 22304

Submitted to:

Naval Research Laboratory
Washington, D. C. 20375

UNCLASSIFIED

SECURITY CLASSIFICATION OF THIS PAGE (When Data Entered)

REPORT DOCUMENTATION PAGE

READ INSTRUCTIONS BEFORE COMPLETING FORM

(14) 1. REPORT NUMBER: JAYCOR-TPD200-80-003-FR

2. GOVT ACCESSION NO.: AD-A083 702

3. RECIPIENT'S CATALOG NUMBER: (9)

4. TITLE (and Subtitle): (6) Final Report on Axial and Radial Compression of Ion Beams.

5. TYPE OF REPORT & PERIOD COVERED: Final Report. 15 Jan 79-26 80, 1/15/79 - 2/26/80

6. PERFORMING ORG. REPORT NUMBER: TPD200-80-003-FR

7. AUTHOR(s): (10) Shyke A. Goldstein, Paul F. Ottinger

8. CONTRACT OR GRANT NUMBER(s): (15) N00173-79-C-0420

9. PERFORMING ORGANIZATION NAME AND ADDRESS:
JAYCOR
205 S. Whiting Street
Alexandria, VA 22304

10. PROGRAM ELEMENT, PROJECT, TASK AREA & WORK UNIT NUMBERS:

11. CONTROLLING OFFICE NAME AND ADDRESS:
Naval Research Laboratory
Washington, DC 20375

12. REPORT DATE: (11) Mar[illegible]80

13. NUMBER OF PAGES: 109 (12) 101

14. MONITORING AGENCY NAME & ADDRESS (if different from Controlling Office):
Naval Research Laboratory
Washington, D. C. 20375

15. SECURITY CLASS. (of this report): UNCLASSIFIED

15a. DECLASSIFICATION/DOWNGRADING SCHEDULE:

16. DISTRIBUTION STATEMENT (of this Report)

1 Copy Code 6700
1 Copy Code 6702
1 Copy Code 6770
12 Copies Defense Documentation Center

17. DISTRIBUTION STATEMENT (of the abstract entered in Block 20, if different from Report)

18. SUPPLEMENTARY NOTES

19. KEY WORDS (Continue on reverse side if necessary and identify by block number)

20. ABSTRACT (Continue on reverse side if necessary and identify by block number)

DD FORM 1 JAN 73 1473 EDITION OF 1 NOV 65 IS OBSOLETE

393453

UNCLASSIFIED

SECURITY CLASSIFICATION OF THIS PAGE (When Data Entered)

CONTENTS

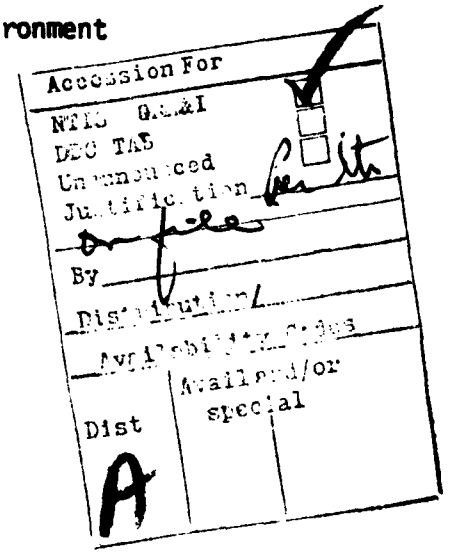

I. INTRODUCTION

In the last year the national program of particle beam drivers for Inertial Confinement Fusion (ICF) has been shifted from Relativistic Electron Beams (REB) to light ion beams. The major reasons for preferring ion beams were the high efficiency of generating them using present pulsed power generators coupled to ion diodes, focusing and transporting the beams, and bunching them in plasma channels. Many of these results have been achieved by the NRL program supported by JAYCOR. In particular, we have proposed the possibility of increasing the power of the ion beam by reducing the pulse length from the 100 ns to 20 or 10 ns needed for ICF targets.

In the present report we concentrate on the physics of propagating intense ion beams in plasma channels. In particular, ~~we have studied~~ the theoretical aspects are studied of the possible effects during ion beam transport on the structure of electromagnetic fields in the plasma. The ion orbits were solved for different classes of plasma channels including bumpy ones in order to evaluate the sensitivity of beam losses due to channels that deviate from idealistic shapes. The consideration of different plasma instabilities, the hydrodynamic motion of the plasma, propagation in filamentary channels and beam energy losses put realistic limits on how much ion current can be propagated using the simple steady plasma channel concept. Axial bunching of the beam (via time dependent voltage ramping of the ion diode) was analyzed and found to be a sound concept as long as no more than an order of magnitude pulse compression is attempted. The radial compression is viable on a small scale in tapered channels (giving a factor of 2 increase in current density) and on a large scale if self magnetic fields fully penetrate the media (giving rise to an order of magnitude increase in ion beam current density). Further theoretical investigation on the details of the next

above mechanisms are presently in progress including new plasma channel schemes that help to push upwards the limits on the ion currents.

II. SUMMARY OF WORK

The theoretical studies were performed along the same approach as envisioned in the proposal with additions that further clarify each subject.

1. In the area of beam-plasma instability, the following results were obtained:

   a. The initial plasma current was found to be about 50 kA for present ion beams. The gas deuterium was shown to be preferential to hydrogen with the needed density 10^{-5} g/cm^3.

   b. The electromagnetic Weibel and Whistler modes were studied and found to be unstable; however, they do not grow fast enough to seriously affect beam transport.

   c. In the transport channel, where electrostatic modes are collisionally stabilized, these electromagnetic modes are the most dangerous instabilities. But for lower plasma densities and higher temperatures the electrostatic modes are the fastest growing.

2. Ion Beam Bunching.

   a. The ion beam energy fluctuations cause pulse broadening but power multiplication by a factor of 5 is easily obtainable.

   b. Ion orbits in filamented channels have been studied resulting in limits on the tolerable level of jitter in the ion beam current density profile. If these limits are violated, beam transport will be affected, particularly at the tail of the beam.

c. Exploring the phase space picture of the ion orbits as defined at the initial injection point leads to conditions for minimizing the amount of beam rippling in the channel. Voltage ramping, ion scattering during transport and non-ideal magnetic field profiles all decrease the usual ripple phase-mixing distance.

d. The optimum plasma and beam parameters for transport of a given current density ion beam have been identified to have injection angles $\alpha < 0.2$ (values of $\alpha \approx 0.1$ are preferable but difficult to achieve) and ion currents of less than 1 MA in the 1 cm^2 channels studied. The major limit on bunching is not α but voltage fluctuations.

3. Radial Compression of Ion Beams.

a. Studying ion orbits in a tapered z-discharge plasma channel has indicated that radial compression of the beam used in conjunction with bunching can enhance bunching power multiplication by at most a factor of 1.3.

b. The ion orbits computed in the steep gradient magnetic fields (generated by either imploding plasma channels or expanding ones) are similar to those of constant current profiles in the plasma but need somewhat larger current for confinement. The major result is that one has to start with initial current above the initial minimum current required for confinement, since plasma expansion sweeps out the linear magnetic field with it generating steep gradients.

c. The self fields and ion orbits were determined for the case where current neutralization does not occur. Focusing at a

distance shorter than a quarter of a betatron wave length was found. The self focusing increased the current density by more than a factor of ten.

d. The sheet ion beam converging in cylindrical geometry with a center line of symmetry and a plane perpendicular to the line with anti-symmetric magnetic fields was shown to follow a similar ion orbit pattern to the tapered z-discharge (3a) but with an additional current density increase of r^{-1}. It may prove useful in final focusing near the pellet.

III. THEORY OF ION BEAM BEHAVIOR IN PLASMA CHANNELS

We first discuss the beam-plasma instabilities in a given plasma channel describing our basic considerations for choosing the specific set of initial plasma parameters.

1. Beam-Plasma Instabilities.

The initial values of the MHD fields are dictated by the fact that the ion beam was assumed to have about 1 cm^2 cross section that is a little smaller than the confining low density plasma. The plasma was chosen to be hydrogen (or deuterium that has twice the mass density for the same plasma density number of electrons) and is fully ionized in the channel. The needed plasma current is about 50 kA, enough to confine 5 MeV protons with spot size $\sqrt{2}$ smaller than the plasma channel and injection angle of 0.15 radians. Since the plasma stopping power is (when fully ionized) $10^3/V_i$ MeV/g/cm^2, where V_i-ion energy in MeV, and since propagation over distances of 5 meters may be necessary hydrogen densities less than 4×10^{18} cm^{-3} should be used for less than 10% energy loss. At the same time the hydrogen density cannot be decreased by large numbers to say 10^{17} cm^{-3} since the plasma expansion is too rapid for ion beam current densities of $J_i = 0.5$ MA/cm^2. The plasma expansion is computed from $J_p \times B$, the pressure induced by the return current $J_p \approx - J_i$. This gives an equation for the radial velocity V_r,

$$\rho \frac{dV_r}{dt} = \frac{J_p \times B}{c} \approx \frac{J_i \times B}{c} ,$$

where ρ is the plasma density (g/cm^3). For a linear estimate

$$V_r = \frac{J_i Bt}{\rho c}$$

which implies that a 10^{17} cm^{-3} hydrogen plasma reaches a velocity of 10^8 cm/s during t = 50 ns for B = 2 x 10^4 Gauss (I = 50 kA, r = 0.5 cm). This expands the plasma radius beyond 2 cm and thus ion beam current density reduction by a factor 16 will occur. In addition, very large return current electric fields due to plasma motion (if $\sigma \to \infty$ the electric field is given by $E = -\frac{V_r \times B}{c} > 10^4$ V/cm) cause unacceptable energy losses (all 5 MeV are lost in 5 meters of transport for the above example). Thus, hydrogen density must exceed 1 x 10^{16} cm^{-3}.

An initial plasma temperature of a few eV is obtained in equilibrium for a 50 kA channel current. The heating of the channel electron to 50 eV is due to the plasma stopping power (resistive heating is negligible). The ion beams were thus studied in the above parameter regimes taking into account the effect of different temperatures and different current profiles as the plasma undergoes expansion. The plasma responds to the ion beam on a long hydrodynamic time scale[1] and on a short, velocity phase-space time scale that can excite fast field instabilities. We assume that the two time scales are separated enough that we may treat them with a semi-static approach, computing a Vlasov formalism during different hydrodynamic states. In future work we may resolve the coupling between the two phenomena when no large time separation exists.

Velocity space electromagnetic instabilities, which lead to azimuthal and radial current bunching in the channel, have been studied. In particular, growth rates for the Weibel ($\underline{k}\cdot\underline{B} = 0$, $\underline{k}\cdot\underline{V}_z \neq 0$) and Whistler ($\underline{k} \times \underline{B} \neq 0$, $\underline{k}\cdot\underline{V}_z = 0$) instabilities are derived in Appendix 1. Although electrostatic instabilities typically have larger growth rates than electromagnetic instabilities, here the Weibel and Whistler modes have the fastest growth because of collisional damping of the electrostatic modes.[2]

The plasma electron current is the main driver for the Weibel instability and the ion beam current is the main driver for the Whistler instability. Both instabilities have relatively slow growth rates so that, at most, 1-2 e-folds occur during beam passage for typical systems. Nonlinear saturation probably is not reached during the beam propagation time, however, the late time level of current bunching can be estimated using the predicted e-folding numbers and the initial perturbations in the system. Such perturbations are most likely produced by jitter in the beam current density (see Appendix 2). Since both instabilities are nonconvecting, beam ions generated at the tail of the pulse are most affected by the current bunching.

2. Ion Beam Bunching.

The effect of diode voltage fluctuations is to set up a variation around the ideal voltage shape and since the ion velocity is $v_i \sim V^{1/2}$, one finds that

$$\frac{\delta v_i}{v_i} = \tfrac{1}{2} \frac{\delta V}{V} \quad .$$

The spread in arrival times to the target is derived from $L = v_i t_a$ where $\delta(v_i t_a) = 0$. Thus

$$\frac{\delta t}{t_a} = - \frac{\delta v_i}{v_i} = - \tfrac{1}{2} \frac{\delta V}{V} \quad .$$

Here L is the target distance and t_a is the arrival time on target. The arrival time is related to the pulse time by a simple relation to the L required for voltage ramping by the amount ΔV during the beam pulse time t_{pulse}:

$$L = 2v_i \left(\frac{V}{\frac{dV}{dt}}\right) \sim 2v_i \left(\frac{V}{\frac{\Delta V}{t_{pulse}}}\right) \quad .$$

Using now $L = v_i\, t_a$ we find that

$$t_a = \frac{2V}{\Delta V}\, t_{pulse} \cdot$$

The result for the broadening of arrival times is that

$$\delta t = \frac{V}{\Delta V}\ \frac{\delta V}{V}\ t_{pulse} \cdot$$

Since one typically ramps the voltage by $\Delta V \leq \frac{1}{2}V$ and since the power multiplication is given by $M = \frac{t_{pulse}}{\delta t}$ one finds that

$$2M \frac{\delta V}{V} \leqslant 1.$$

The spread in arrival time due to betatron orbits is found by comparing motion of ions on axis moving at full $v_z = v_i$ with ions with finite α moving at $v_z = (v_i^2 - v_r^2)^{\frac{1}{2}}$, where $v_r = v_i \alpha \cos \omega_B t$. For small α

$$v_z = v_i(1 - \tfrac{1}{2}\, \alpha^2 \cos^2 \omega_B t) \ .$$

Averaging over one betatron orbit, $< v_z > = v_i(1 - \frac{1}{4}\, \alpha^2)$. This gives a change in arrival time of $\delta t = \frac{1}{4}\, \alpha^2\, t_a \geq \alpha^2\, t_{pulse}$ which for $\alpha = 0.1$ is only 0.01 of the original pulse length adding 10% to a beam bunched by $M = 10$. Even for $\alpha = 0.2$ this adds only 40% pulse broadening (for $M = 10$). We thus conclude that power multiplication by factors of 5 is an easy task since only about 10% accuracy in voltage shaping is required and no significant effect is expected from betatron orbit lengthening for $\alpha \leq 0.2$.

Ion beam propagation in a filamented channel is investigated in Appendix 2. The filamentation is a result of either radial or azimuthal current bunching produced respectively by either the Weibel or Whistler instability. In both cases the results of analysis set limits on the initial level of jitter in the beam current density. If the initial jitter surpasses these limits, beam transport will be affected. When operating above the radial current bunching limit, the beam will either be expelled from the center of the channel or be pinched into the center of the channel depending on the phase of the initial perturbation. When operating above the azimuthal current bunching limit, the beam is depleted in time as increasingly more ions are lost to the dense plasma surrounding the channel. Typically, these current bunching limits are not expected to be reached so that good transport is anticipated. If higher current levels than expected are reached, only the tail of the beam will be affected since the modes are nonconvecting.

Coherent rippling of the radial beam envelope is investigated in Section III of Appendix 3. This phenomenon is easily understood by exploring the phase space picture of the ion betatron orbits as defined by the initial injection conditions. In the absence of other mechanisms, the rippling eventually phase mixes out after many ripple wavelengths due to the weak dependence of the betatron frequency on the small spread in ion injection angles. Other mechanisms, such as voltage ramping, steep gradients in the magnetic field profile ($B_\theta \sim r^n$ for $n > 1$) and ion scattering during trasnport can considerably reduce this phase mixing distance. In order to minimize variations in the beam radius, $r_b(z)$, at the beginning of the transport channel, the channel should be matched as well as possible to the beam. This is accomplished by setting the betatron frequency equal to

$v_i\alpha_m/r_s$ where v_i is the beam velocity, α_m is the maximum injection angle, and r_s is the beam spot size.

At the end of the transport channel the phase mixed density profile for the ideal (B_θ—r) magnetic field profile shows a strong peak on axis, varing like r^{-1} as $r \to 0$. The addition of beam angular momentum reduces the central density, however the beam density profile will remain peaked on axis since minimal azimuthal ion motion is observed in shadow-box experiments.

Given the information obtained from this work, one can arrive at a set of optimized plasma and beam parameters for transport of a given current density beam. Eqs. (11) and (27) of Appendix 3 set upper and lower limits on the required channel current. Eq. (11) states that the channel current must be large enough to confine the beam and Eq. (27) states that the channel current cannot be so large as to produce a large degree of beam rippling. The electromagnetic instability analysis sets limits on beam quality (Eqs. (13) and (26) of Appendix 2). The electrostatic instability analysis gives a lower limit on the plasma density (Eqs. (11) and (31) of Ref. 2) where the limit depends on beam parameters and the plasma electron temperature. MHD code work provides $T_e(n_p)$ for a given beam. MHD considerations also provide a lower limit on the plasma density from plasma expansion consideration as discussed earlier in Sec. III-1.

The ideal target irradiation time and the initial beam pulse duration determine the required bunching factor which in turn specifies the channel length for a given voltage ramp. The required bunching factor also sets an upper limit on the spread in ion beam injection angles (Eq. (14) of Appendix 3) and a limit on the variation of the actual voltage ramp from the ideal ramp.[3]

3. Radial Compression of Ion Beams.

The radial compression of ion beam current density was investigated for the possibility of using either self magnetic fields or externally applied ones. In general, the gain in current density is obtained at the expense of turning a relatively cold beam into a hot one. In principle, for any given beam there will exist a given structure that may bring about the highest radial compression possible into a given focus. Since reality sets limits on the possibility of constructing such fields we have considered in the present studies rather simple geometries and divided them into two classes: self fields and external fields. The case of steep radial (and/or axial) gradients shows confinement and radial compression if currents beyond those needed for uniform current distribution are driven in the plasma. The basic orbits were studied in Appendices 2 and 3. Based on these results, recent studies in that direction may provide easy experimental ways of gaining factors of 4 radial area compression; these studies are presently being pursued. We now turn to the weak gradient case.

In order to investigate the value of radial beam compression, ion orbits in a tapered z-discharge channel were studied (Section IV, Appendix 3). A multiple scales analysis was used in order to properly treat the slowly decreasing channel radius. Although the amplitude of the ion betatron orbit does decrease as the ion propagates down the tapered channel, the amplitude decreases slower than the channel radius. Thus, the effectiveness of radial compression is limited. When used in conjunction with axial bunching, radial beam compression can enhance bunching power multiplication by a factor of 1.3.

The self magnetic field radial compression was also studied. In the case of a fully non-current-neutralized ion beam the ion orbits were computed in the self-consistent magnetic field assuming zero electric field. The

ions are assumed to enter through an entrance foil with small transverse kinetic energy. As these orbits converge, the magnetic field along particle orbits increases as r^{-1} as long as no particle orbit crossing occurs. This is justified for the case of a uniform current distribution (see Appendix 4), and total ion current much less than the Alfven current ($I_A = 3.1 \times 10^7 \beta_i$ amperes) and radial compression ratios of 5 giving current density increases of 25 before the cold flow breaks down. In future studies, attempts may be made at a Vlasov formalism that includes particle orbit crossing in order to see how much compression may be obtained. In addition, realistic time dependent effects, such as different current profiles, voltage variations, inductive electric fields and finite rise time of magnetic fields should be studied.

When a converging sheet ion beam was treated in a cylindrical geometry using magnetic field structures that have azymuthal symmetry but are anti-symmetric with respect to a plane perpendicular to the axis of symmetry, it was found to be very similar to the tapered z-discharge. The reason for that is the antisymmetric current flow which, after converging to the axis, is divided into two halves, each going in opposite directions through the two poles. The $\underline{B}$ field thus goes as r^{-1} and drops linearly inside the plasma. Ion orbits thus converge geometrically like r^{-1} and in addition, are compressed by the same effect as in the radially compressed beam in the tapered z-pinch.

Future theoretical work in this area of ion beam focussing, transport and bunching will expand on the work presented here. In particular, work is in progress studying new plasma channel schemes that help to push upwards the limits on deliverable ion currents.

IV. REFERENCES

1. D. Mosher, G. Cooperstein, Shyke A. Goldstein, D. G. Colombant, P. F. Ottinger, F. L. Sandel, S. J. Stephanakis, and F. C. Young in Proceedings of the 3rd International Topical Conference on High Power Electron and Ion Beam Research and Technology, Novosibirsk, USSR (1979).

2. P. F. Ottinger, D. Mosher, and Shyke A. Goldstein, Phys. Fluids 22, 332 (1979).

3. D. Mosher, Shyke A. Goldstein, Bull. Am. Phys. Soc. 23, 800 (1978).

V. APPENDICES

APPENDIX 1. Electromagnetic Instabilities in a Focused Ion Beam Propagating Through A Z-Discharge Plasma.

ELECTROMAGNETIC INSTABILITIES IN A FOCUSED ION BEAM PROPAGATING THROUGH A z-DISCHARGE PLASMA

I. INTRODUCTION

In an earlier paper,[1] it was shown that focused ion beams for use in a pellet fusion device can propagate axially down a z-discharge plasma channel without generating disruptive microturbulence due to electrostatic streaming instabilities. The azimuthal magnetic field in the z-discharge channel confines the beam radially as it propagates. Here the analysis will be extended to study electromagnetic velocity-space instabilities. In particular, the Weibel instability ($\mathbf{k} \cdot \mathbf{B} = 0$, $\mathbf{k} \cdot \mathbf{V}_z \simeq 0$) and the Whistler instability ($\mathbf{k} \times \mathbf{B} \simeq 0$, $\mathbf{k} \cdot \mathbf{V}_z \simeq 0$) are investigated, where $\mathbf{k}$ is the wavevector, $\mathbf{B}$ is the azimuthal magnetic field and $\mathbf{V}_z = V_z \hat{e}_z$ is the axial streaming velocity of the beam.

The beam-plasma system consists of a focused ion beam (typically a 5 MeV proton beam of 50 ns duration, 0.5 cm radius, and a current of $5 \times 10^5 A$) propagating down the axis of a z-discharge plasma channel.[2] The ion beam is focused at the entrance to the plasma channel (see Figure 1) with velocity components transverse to z given by $V_\perp / V_z \simeq \tan \theta << 1$. A high plasma density in the channel ($n_p \simeq 10^{18}\,\mathrm{cm}^{-3}$) insures good beam charge neutralization.[3] Good beam current neutralization in the interior of the beam also occurs, so that the total magnetic field is comparable to that associated with the preformed channel established before beam injection. The beam current greatly exceeds that establishing the channel so the electron drift velocity is approximated by $V_e \simeq n_b V_z / n_p$.

Manuscript submitted August 6, 1979.

Hydrodynamic modeling of the background plasma[4] shows that a uniform channel net-current model is appropriate for the early times associated with passage of the beam front. This is because the low-temperature channel is established microseconds before beam injection so that complete magnetic diffusion occurs. Later in the ion pulse, expansion of the beam-heated high-temperature plasma ($T \simeq$ 25-50 eV) reduces the magnetic field strength in the interior of the channel. The built-up field in the expanding cylindrical shock wave is also enhanced by significant current non-neutralization in the cool plasma surrounding the beam-heated channel. The maximum field strength just outside the ion-beam radius can exceed that established by the initial z-discharge current by a large factor. Thus, at late times during beam passage, the magnetic field distribution is closely approximated by a surface-current model.

In Sec. II, equilibrium models for such a beam plasma system will be described. In Secs. III and IV, the Wiebel and Whistler instabilities will be investigated. The conclusions which can be drawn from this work are summarized in Sec. V.

II. BEAM-PLASMA EQUILIBRIUM

For mathematical convenience, a slab model will be used for the beam-plasma system. This is appropriate for the case at hand since ions are injected into the channel with small angular momentum so that the resulting orbital motion occurs in a plane. At early times in the pulse, the net current (nearly equal to the channel current) is uniformly distributed across the channel and flows in the z direction. Thus, $\mathbf{B} = B_y \hat{e}_y$ where

$$B_y = \begin{cases} B_p x/a, & |x| < a \\ B_p, & |x| > a \end{cases} \tag{1}$$

Here, B_p is the peak value of the field and "a" is the channel radius. If the beam distribution function f_b is written as

$$f_b(v_x, v_y, v_z) = \frac{n_b}{\pi} \delta(v_y)\, \delta\left(v_x^2 + v_z^2 - \frac{2V_z P_z}{m_i} + K\right) \tag{2}$$

where $P_z = m_i v_z + eA_z/c$ is the axial canonical momentum, A_z is the vector potential and n_b, V_z and K are constants, then

$$n_b(x) = \begin{Bmatrix} n_b, & |x| < r_b \\ 0, & |x| > r_b \end{Bmatrix}, \tag{3}$$

where $r_b = V_\beta/\omega_o$, $K = V_z^2 - V_\beta^2$, $\omega_o^2 = V_z\bar{\omega}_{ci}/a$ and $\bar{\omega}_{ci} = eB_\theta/m_i c$. A smoothly falling density profile may be obtained by replacing the second delta function in Eq (2) by a Maxwellian distribution function. The distribution function in Eq. (2) also states that all beam ions cross the axis at the same angle and traverse the entire beam radius during each betatron oscillation. A more complicated distribution function could be used to model the small spread in angles at which the ions cross the axis, however little additional information is obtained for the effort. For mathematical convenience, the form of the distribution function given in Eq (2) will be used here. It is easy to show that the fluid velocity is given by $\mathbf{V} = V_z\hat{e}_z$ and that in order for the beam to be confined within the plasma channel, one must have $r_b \leqslant a$. Furthermore, f_b can be written in the more convenient form

$$f_b(v_y, v_\beta, \phi) = \frac{n_b}{\pi}\,\delta(v_y)\,\delta(v_\beta^2 - V_\beta^2 + \omega_o^2 x^2), \tag{4}$$

where $v_x \equiv v_\beta \sin\phi$, $v_z \equiv V_z + v_\beta\cos\phi$ and $v_\beta^2 = v_x^2 + (v_z - V_z)^2$. Here, V_z is associated with the average streaming velocity of the beam ions and v_β is associated with the oscillatory betatron motion of the beam ions ($v_\beta \leqslant V_\beta = \omega_o r_b$). The beam-ion orbit equations for this field geometry were solved in Ref. 1 and the results are summarized in Appendix A.

The distribution function given in Eqs. (2) or (4) provides an appropriate discription of the ion beam at early times in the pulse. At late times $B_y = 0$ inside the channel and the field is built-up sharply at the radial edge of the beam. Thus at late times in the pulse

$$f_b(v_y, v_\beta, \phi) = \begin{Bmatrix} \frac{n_b}{\pi}\,\delta(v_y)\,\delta(v_\beta^2 - V_\beta^2), & |x| < r_b \\ 0, & |x| > r_b + \delta \end{Bmatrix}. \tag{5}$$

where $B_y(r_b + \delta)$ is sufficiently large to confine the beam and the sheath is restricted to a thin layer such that $\delta << r_b$. Beam ions move in straight line orbits inside the field-free channel. Within the layer $\gamma_b < |x| \leq \gamma_b + \delta$, the ions reflect off the magnetic wall, reverse their transverse velocity and resume their straight line trajectories after reentering the channel. The distribution function in Eq. (5) also results in the uniform density profile of Eq. (3) and in a fluid velocity given by $\mathbf{V} = V_z\hat{e}_z$ inside the channel.

The background plasma provides complete charge and nearly complete current neutralization of the beam. In addition, the plasma also carries the z-discharge current. The high density desired for good beam neutralization provides for a high frequency of electron-plasma ion collisions, ν_e, shown[4] to be larger than ω_{ce} inside the channel at all times during the pulse. Thus, a collisional fluid model is used for the background plasma with the electrons drifting with velocity $\mathbf{V}_e \simeq (n_b V_z/n_p)\,\hat{e}_z$.

III. THE WEIBEL INSTABILITY

Two Weibel instabilities will be investigated, the ion instability and the electron instability, which are respectively driven by the streaming of the beam ions and the electron drift motion. Lee and Lampe[5] report for electron beams that the Weibel instability grows at a greatly reduced rate when $V_\perp/V_z > \omega_{pb}/\omega_{pe}$ where ω_{pb} is the beam plasma frequency and ω_{pe} is the electron plasma frequency. Molvig[6] has shown that is possible for electron-ion colisions to restore rapid growth of the mode. Although the concern here is with ion beams driving the instability, again both beam-thermal effects and collisional effects are important. Ion betatron motion will also be important in analyzing the ion instability.

A. Ion Instability

Consider first the situation late in the beam pulse, with f_b given by Eq. (5). For assumed large r_b, the perturbed distribution function with $\mathbf{E}(\mathbf{x}) = \mathbf{E}\exp(ikx)$,

$$f_{b1} = \frac{-e}{m_i}\int_{-\infty}^{0} d\tau\left[\mathbf{E} + \frac{\mathbf{v}\times\mathbf{B}}{c}\right]\cdot\frac{\partial f_b}{\partial \mathbf{v}}\exp i(k\mathrm{v}_x - \omega)\,\tau, \tag{6}$$

can be integrated over τ to give

$$f_{b1} = \left[\frac{-ie/m_i}{\omega - k\mathrm{v}_x}\right]\left[\left(E_x + \frac{k\mathrm{v}_z}{\omega}E_z\right)\frac{\partial f_b}{\partial \mathrm{v}_x} + \left(1 - \frac{k\mathrm{v}_x}{\omega}\right)E_z\frac{\partial f_b}{\partial \mathrm{v}_z}\right]. \tag{7}$$

Here $\mathbf{k} = k\hat{e}_x$ and straight-line unperturbed orbits are used since $B_y = 0$ for $|x| < r_b$. The assumption that $n_b/n_p << 1$ allows one to write the usual approximate dispersion equation,[6] $D_{zz} \approx 0$, for the Weibel instability where $|\omega| < \nu_e$ and

$$D_{zz} \approx 0 = c^2k^2 + \gamma^2 + \omega_{pi}^2\gamma/\nu_i + I_{zz}. \tag{8}$$

Here $\omega = i\gamma$ for purely growing perturbations,[6] $\nu_i = m_e\nu_e/m_i$, $V_z >> V_e$ (electron drift motion is ignored at present) and I_{zz} is the beam contribution to D_{zz};

$$I_{zz} = \frac{-4\pi e^2}{m_i}\int\left[\left(\frac{k\mathrm{v}_z^2}{i\gamma - k\mathrm{v}_x}\right)\frac{\partial f_b}{\partial \mathrm{v}_x} + \mathrm{v}_z\frac{\partial f_b}{\partial \mathrm{v}_z}\right]d^3\mathrm{v}. \tag{9}$$

Integrating by parts and then using the calculus of residues to perform the remaining nontrivial integration results in

$$I_{zz} = \frac{\omega_{pb}^2\gamma}{k^2V_\beta^2}\left[\frac{k(V_\beta + 2V_z)}{(1 + \gamma^2/k^2V_\beta^2)^{1/2}} - \frac{2k^2V_zV_\beta}{\gamma} - \frac{kV_z^2/V_\beta}{(1 + \gamma^2/k^2V_\beta^2)^{3/2}}\right] \tag{10}$$

which reduces to

$$I_{zz} = \begin{cases} -\omega_{pb}^2\left[\dfrac{2V_z}{V_\beta} + \dfrac{V_z^2\gamma}{kV_\beta^3}\right], & \gamma << kV_\beta \\ -\omega_{pb}^2\left[1 - \dfrac{k^2V_z^2}{\gamma^2}\right], & \gamma >> kV_\beta \end{cases}. \tag{11}$$

for $V_z > V_\beta$ and the limits shown. Solving Eq. (8) for the growth rate, γ, one obtains

$$\gamma = \begin{cases} (k^2 V_z^2 \nu_i \omega_{pb}^2/\omega_{pi}^2)^{1/3}, & 0 < k < k_p \\ \left(\dfrac{2\omega_{pb}^2 \nu_i V_z}{\omega_{pi}^2 V_\beta}\right)\left(1 + \dfrac{2\omega_{pb}^2 V_z^2 \nu_i}{\omega_{pi}^2 k V_\beta^3}\right), & k_p < k < k_o \\ 2\omega_{pb} c (2V_z/V_\beta)^{1/2} (k_o - k), & k \simeq k_o \end{cases}, \tag{12}$$

where

$$k_p = (\omega_{pb}^2 \nu_i V_z^2/2^{3/2}\omega_{pi}^2 V_\beta^3); \quad k_o = (\omega_{pb}/c)\ (2V_z/V_\beta)^{1/2}.$$

The peak growth rate is given by

$$\gamma_p^i = \frac{\omega_{pb}^2 \nu_i}{\omega_{pi}^2}\left(\frac{2V_z^2}{V_\beta^2}\right)^{4/5} \quad \text{at} \quad k = k_p. \tag{13}$$

For $n_b/n_p \sim 10^{-3}$ and $V_\beta/V_z \gtrsim 10^{-1}$, $\gamma_p^i \sim 10^6$ sec^{-1} at late times in the beam pulse (note that γ_p^i is actually overestimated here since $k_p r_b << 1$). Thus, no significant growth can occur since $\gamma_p^i \tau_b \gtrsim 0.05$; here τ_b is the beam pulse length.

At early times in the beam pulse, ν_i is larger due to low channel temperatures so that one might expect the growth rate to be larger. It will be found, however, that by including the betatron motion of beam ions in the analysis, the perturbation is stabilized. In this case, f_b is given by Eq. (4), the ion orbits are found in Appendix A, and f_{b1} is given by

$$f_{b1} = \frac{-2e}{m_i}\frac{\partial f_b}{\partial v_\beta^2}\int_{-\infty}^{0} d\tau \Big[v_x' E_x(x') + (v_z' - V_z)\ E_z(x') \Big[-\frac{iV_z v_x'}{\omega}\frac{\partial E_z}{\partial x'}\Big] \exp(i\omega\tau) \tag{14}$$

It is now assumed that $E_z(x) \simeq \bar{E}_z \cos kx$ where k is restricted to a discrete set of values by boundary conditions at r_b with $kr_b \gtrsim 1$. This choice of $E_z(x)$ is reasonble since n_p and n_b are both uniform and $n_b << n_p$. Thus, the mode is expected to closely resemble the background plasma eigenmode which is sinusoidal. Here again, the background plasma is treated as

a collisional fluid since $\nu_e > \omega_{ce}$. An approximate algebraic dispersion equation is obtained by taking a weighted spatial average of $\hat{D}_{zz}E_z(x)$ where $\hat{D}_{zz}$ is a differential operator in x defined by

$$\hat{D}_{zz} = -c^2\frac{\partial^2}{\partial x^2} + \gamma^2 + \frac{\omega_{pi}^2\gamma}{\nu_i} - 4\pi ie\int v_z f_{b1} d^3v$$

and f_{b1} is given in Eq. (14) ($E_x \approx 0$). The dispersion equation is then

$$0 \approx \bar{D}_{zz} \equiv \frac{1}{r_b\bar{E}_z}\int_{-r_b}^{r_b} dx\ \hat{D}_{zz}E_z(x)\cos kx \tag{15}$$

Using the orbit equations for x′ and v′ found in Appendix A and the Bessel function identities

$$\exp(\pm\, iz\sin\theta) = J_o(z) + 2\sum_{l=1}^{\infty} J_{2l}(z)\cos 2l\theta$$
$$\pm\, 2i\sum_{l=0}^{\infty} J_{2l+1}(z)\sin(2l+1)\,\theta, \tag{16}$$

and

$$\exp(iz\cos\theta) = J_o(z) + 2\sum_{l=1}^{\infty} i^l J_l(z)\cos l\theta, \tag{17}$$

the τ integration in Eq. (14) can be performed. Thus, Eq. (15) takes the form

$$0 = c^2k^2 + \gamma^2 + \frac{\omega_{pi}^2\gamma}{\nu_i} + \bar{I}_{zz} \tag{18}$$

where in terms of $\alpha_1(x, v_x, v_z)$ and $\alpha_2(x, v_x, v_z)$

$$\bar{I}_{zz} = \frac{-2\omega_{pb}^2}{n_b}\int_{-r_b}^{r_b} dx\cos kx\int d^3v\, v_z\frac{\partial f_b}{\partial v_\beta^2}\left[\frac{kV_z}{\gamma}\alpha_1 + \alpha_2\right]. \tag{19}$$

The expressions for α_1 and α_2 are given in Appendix B. Terms involving resonances at higher harmonics of ω_o [i.e. $(\omega - m\omega_o)^{-1}$ for $m \neq 0$] are not considered. The term involving α_1 in Eq. (19) is the source of instability. Here, however, because of the betatron motion, this term vanishes and the mode is stable at early times in the pulse (see Appendix B). This same result is obtained for odd eigenfunctions, $E_z(x) = \bar{E}_z \sin kx$. Mathematically the term vanishes because the integrand involving α_1 is an odd function of x (see Appendix B). Physically no

radial current bunching can occur since each ion travels radially back and forth across the beam profile as it follows its betatron orbit. However, azimuthal current bunching can occur as will be discussed in Sec. IV.

B. Electron Instability

The only other source of energy available to drive the Weibel instability at early times in the pulse is the drifting electron background. The drift velocity, however, is actually subthermal since even before beam heating occurs $V_e \simeq n_b V_z/n_p < u_e = (T/m_e)^{1/2}$. Using a warm collisional model ($\nu_e > \omega_{ce}$ at all times), the dispersion equation for the electron-Weibel instability is derived in Appendix C. Setting $\gamma = 0$ in Eq. (C7), it is found that $\gamma > 0$ for $0 < k < k_o = \omega_{pi} V_e/\sqrt{2} u_i c$, where $u_i = (T/m_i)^{1/2}$. Thus for $k < k_o$ and $\omega_{pi}^2 > \gamma \nu_i$, Eq. (C8) reduces to

$$0 = c^2 k^2 + \frac{\omega_{pi}^2 \gamma}{\nu_i} - \frac{\omega_{pi}^2 k^2 V_e^2 (\gamma^2 + \nu_i \gamma + k^2 u_i^2)}{(\gamma^4 + \nu_i \gamma^3 + 3k^2 u_i^2 \gamma^2 + 2\nu_i k^2 u_i^2 \gamma + 2k^4 u_i^4)}, \tag{20}$$

where the ion beam contribution to Eq. (20) is ignorable.

At early times in the pulse, $\omega_{pi} u_i/c\nu_i < 1$ and

$$\gamma = \begin{cases} (k^2 V_e^2 \nu_i)^{1/3}, & 0 < k < \tilde{k}_1 \\ \omega_{pi} V_e/c, & \tilde{k}_1 < k < k_o \\ \dfrac{\sqrt{2}\,\nu_i c V_e}{\omega_{pi} u_i} (k_o - k), & k \approx k_o \end{cases}, \tag{21}$$

where $\tilde{k}_1 = (\omega_{pi}/c)\,(\omega_{pi} V_e/c\nu_i)^{1/2}$. Here $T \approx 4$ eV, $n_p \simeq 2 \times 10^{18}\,\mathrm{cm}^{-3}$ and $n_b/n_p \simeq 5 \times 10^{-4}$, so that the peak growth rate is on the order of $\gamma_p = \omega_{pi} V_e/c = 4.2\tau_b^{-1}$.

At later times in the pulse, the beam has heated the plasma; then $\omega_{pi} u_i/c\nu_i > 1$ and

$$\gamma = \begin{cases} (k^2 V_e^2 \nu_i)^{1/3}, & 0 < k < k_1 \\ V_e^2 \nu_i/2u_i^2, & k_1 < k < k_2 \\ \dfrac{kV_e}{2}\left[1 - \dfrac{2k^2 c^2 u_i^2}{\omega_{pi}^2 V_e^2}\right]^{1/2}, & k_2 < k \leq k_o \end{cases}, \tag{22}$$

where $k_1 = \nu_i V_e^2/u_i^3$, $k_2 = \nu_i V_e/u_i^2$ and $V_e \lesssim u_i$. Now $\gamma_p^e = \omega_{pi} V_e^2/(2^{3/2} c u_i) \simeq 1.0\tau_b^{-1}$ for $T \simeq 38$ eV, $n_p \sim 1 \times 10^{18}$ cm^{-3} and $n_b/n_p \sim 1 \times 10^{-3}$. Thus, $\gamma_p^e \tau_b$ decreases by a factor of four as the beam passes through and heats the plasma. In fact, $\omega_{pi} u_i/c\nu_i = 1$ at $t \simeq 10.0$ ns into the pulse so that a total of about 1.6 e-folds occur during the transit of the beam.

Note that τ_b is the appropriate time scale for instability growth since $V_e = 0$ except during the passage of the beam. Furthermore, for small k_z (i.e. $k_z^2 < 2\omega_{pi}^2/3c^2$), it can be shown from Eq. (C9) that

$$v_g = \frac{\partial \omega_r}{\partial k_z} = \frac{3k_z^2 V_e^3}{2\gamma_o^2} < V_e << V_z, \tag{23}$$

and

$$\gamma = \gamma_o - \frac{k_z^2 V_e^2}{2\gamma_o}, \tag{24}$$

where $\gamma_o = \omega_{pi} V_{e/c}$. Thus, the unstable mode convects axially, but with a group velocity, v_g, which is much slower than V_z or V_e. At any given point in the plasma the mode grows only for a time of order τ_b. For larger k_z and fixed k_x the mode transforms into the electrostatic streaming instability which was found to be stable in Ref. 1.

C. Summary for the Weibel Instabilities

In summary, it is found that the betatron motion of the beam ions stabilizes the ion-Weibel instability at the beam front while growth is too slow at the tail of the beam to allow for even one e-fold ($\gamma_p^i \tau_b \gtrsim 0.05$). The electron-Weiber instability, on the otherhand, grows fastest ($\gamma_p^e \tau_b \simeq 4.2$) at the front of the beam where the plasma is relatively cold. At the tail of the beam $\gamma_p^e \tau_b \simeq 1.0$. Although the electron-Weibel instability grows faster than the ion-Weibel instability, it also is not expected to grow to a level which could seriously affect beam propagation.

IV. THE WHISTLER INSTABILITY

The Whistler mode ($\mathbf{k} \times \mathbf{B} \simeq 0$, $\mathbf{k} \cdot \mathbf{V}_z = 0$) like the Weibel instability can be driven unstable by particle streaming. However, the wavevector $\mathbf{k} = k_y \hat{e}_y$ (i.e. $\hat{e}_\theta$ in cylindrical geometry) is perpendicular to the direction of the betatron motion of the beam ions. Hence, unlike the Weibel instability, the Whistler instability cannot be stabilized by the beam ion betatron motion. However, a small spread in v_y (angular momemtum) can reduce the growth rate significantly. The electron drift velocity is ignored when considering the ion-Whistler instability since $V_z >> V_\theta$.

Consider first the situation late in the beam pulse with f_b given by Eq. (5). If it is assumed for the moment that r_b is very large, then the perturbed distribution function is given by

$$f_{b1} = \left[\frac{-ie}{m_i}\left(\mathbf{E} + \frac{\mathbf{v} \times \mathbf{B}}{c}\right) \cdot \frac{\partial f_b}{\partial \mathbf{v}}\right] / (\omega - k_y v_y). \tag{25}$$

Using this expression for f_{b1}, the perturbed current is easily calculated and used to derive the dispersion equation,

$$D_{zz} = c^2 k^2 y + \gamma^2 + \frac{\omega_{pi}^2 \gamma}{\nu_i} + \omega_{pb}^2 \left\{1 - \frac{k^2 (V_z^2 + V_\beta^2/2)}{\gamma^2}\right\} \simeq 0. \tag{26}$$

Again $n_b/n_p << 1$ was used in deriving Eq. (26) where $\omega = i\gamma$ for purely growing perturbations and $V_\theta << V_z$ (electron drift motion is ignored at present).

Solving Eq. (26) yields

$$\gamma = \begin{cases} k_y V_z, & 0 < k_y < k_1 \\ (k_y^2 V_z^2 \omega_{pb}^2 \nu_i / \omega_{pi}^2)^{1/3}, & k_1 < k_y < k_2 \\ \omega_{pb} V_z / c, & k_y > k_2 \end{cases}, \tag{27}$$

where

$$V_z > V_\beta; \; k_1 = \omega_{pb}^2 \nu_i / \omega_{pi}^2 V_z; \; k_2 = (\omega_{pi}/c)\,(\omega_{pb} V_z / \nu_i c)^{1/2}.$$

The peak growth rate (for $k_y > k_2 \simeq 25.0\ \text{cm}^{-1}$) is given by $\gamma_p^i = \omega_{pb} V_z/c \simeq 2 \times 10^2\, \tau_b^{-1}$, for a beam with no spread in v_y.

This result is only slightly modified when finite geometry effects and the betatron motion of the beam ions and included. Proceeding as in Appendix B with $\mathbf{k} = k_x\hat{e}_x + k_y\hat{e}_y$ and f_b given in Eq. (4), one obtains

$$D_{rr} = c^2(k_x^2 + k_y^2) + \gamma^2 + \frac{\omega_{pi}^2\gamma}{\nu_i} + \omega_{pb}^2\left[F(k_x r_b) - \frac{k_y^2(V_z^2 + V_\beta^2/2)}{\gamma^2}\, G(k_x r_b)\right], \tag{28}$$

where $F(k_x r_b)$ is defined in Eq. (B6). The quantity $G(k_x r_b)$ is defined by

$$G(k_x r_b) \equiv \frac{2}{k_x N}\int_o^{k_x r_b} \cos X\Big[J_o(X)\, J_o^2(Z) + 2\sum_{n=1}^{\infty} J_{2n}(X)\, J_n^2(Z)\Big]_{Z=\tilde{Z}(X)}\, dX \tag{29}$$

with $X = k_x x$, $\tilde{Z}(X) = (k_x r_b/2)\,(1 - X^2/k_x^2 r_b^2)^{1/2}$ and $N = r_b + (\sin 2k_x r_b)/2k_x$. Note that $G(k_x \simeq 0) = 1$. F and G are only geometrical factors and do not modify the structure of the dispersion equation. For large k_y the peak growth rate now becomes $\gamma_p^i = (\omega_{pb} V_z/c)\,[G(k_x r_b)]^{1/2}$, which, aside from the geometrical correction, is identical to γ_p found in Eq. (27).

If the beam has a small spread in v_y, the beam can be modeled by the distribution function

$$f_b = \frac{n_b}{\pi^{3/2} V_y}\, \delta(v_\beta^2 - V_\beta^2)\, \exp(-v_y^2/V_y^2), \tag{30}$$

where V_y is the thermal velocity of the beam ions. Since the y motion is unaffected by B_y, the distribution in v_y will be the same at all points inside the channel. For convenience finite geometry effects and the effects of the betatron motion of the beam ions are ignored here since they have little affect on the Whistler mode. Substituting the distribution function of Eq. (30) into Eq. (25) yields an expression for the perturbed distribution function, f_{b1}. The perturbed current j_{b1} can then be calculated and the dispersion equation derived.

$$D_{zz} = c^2k^2 + \gamma^2 + \omega_{pi}^2\gamma/\nu_i + I_{zz} \simeq 0. \tag{31}$$

In Eq. (31), $\omega = i\gamma$ and

$$I_{zz} = \frac{\omega_{pb}^2}{\sqrt{\pi}V_y}\int_{-\infty}^{\infty} dv_y\left[1 + \frac{2k_y v_y(V_z^2 + V_\beta^2/2)}{V_y^2(i\gamma - k_y v_y)}\right]\exp(-v_y^2/V_y^2). \tag{32}$$

Here, the v_β and ϕ integrations are trivial and have already been carried out. The quantity I_{zz} is easily written in terms of the usual plasma dispersion function, $Z(\zeta)$[8]. However, here ζ is pure imaginary so that

$$I_{zz} = \omega_{pb}^2\left\{1 - \frac{2V_z^2}{V_y^2}\left[1 - \frac{\sqrt{\pi}\gamma}{k_y V_y}\exp\left(\frac{\gamma^2}{k_y^2V_y^2}\right)\left[1 - erf\left(\frac{\gamma}{k_y V_y}\right)\right]\right]\right\}, \tag{33}$$

where $V_z > V_\beta$ and $erf(x)$ is the usual error function.[9] For $\gamma > kV_y$, Eq. (31) reduces to Eq. (26), but for $\gamma < kV_y$ the dispersion equation becomes

$$0 = c^2k^2 + \gamma^2 + \frac{\omega_{pi}^2\gamma}{\nu_i} + \omega_{pb}^2\left\{1 - \frac{2V_z^2}{V_y^2}\left[1 - \frac{\sqrt{\pi}\gamma}{kV_y} + \frac{2\gamma^2}{k^2V_y^2} + \dots\right]\right\}. \tag{34}$$

From this it is found that the peak growth rate, $\gamma_p = \omega_{pb}V_z/c$, for the case with $V_y = 0$ is reduced if $V_y^2 > 2\nu_i\omega_{pb}cV_z/\omega_{pi}^2$. Since this is the case here

$$\gamma = \begin{cases} kV_z, & 0 < k < k_1 \\ (k^2V_z^2\nu_i\omega_{pb}^2/\omega_{pi}^2)^{1/3}, & k_1 < k < k_2 \\ \dfrac{2\omega_{pb}^2\nu_i V_z^2}{\omega_{pi}^2V_y^2}\left[1 - \dfrac{c^2k^2V_y^2}{2\omega_{pb}^2V_z^2}\right], & k_2 < k \ll k_o \end{cases}, \tag{35}$$

where $k_1 = \omega_{pb}^2\nu_i/\omega_{pi}^2V_z$, $k_2 = k_1V_z^2/V_y^2$ and $k_o = \sqrt{2}\,\omega_{pb}V_z/cV_y$.

The peak growth rate is now

$$\gamma_p' = (\omega_{pb}V_z/c)\ (2\nu_i\omega_{pb}cV_z/V_y^2\omega_{pi}^2) < \omega_{pb}V_z/c,$$

where γ_p' varies in time as $T^{-3/2}(t)$ through ν_i. The number of e-folds, δ during the beam transit at any point in the plasma is given by

$$\delta = \int_0^{\tau_b}\gamma_p'(t)\,dt = \gamma_p'(0)\int_0^{\tau_b}\frac{dt}{(1 + \Delta Tt/\tau_b)^{3/2}}. \tag{36}$$

where it is demonstrated later than no significant wave convection occurs. Here $\Delta T = [T(\tau_b) - T(0)]/T(0)$ for T in eV and $\gamma_\beta'(0)$ is the peak growth rate at the front of the beam. A linear rise in temperature, $T(t)/T(0) = 1 + \Delta T t/\tau_b$, agrees well with results of previous work.[3] Thus

$$\delta = \frac{2\gamma_\beta'(0)\,\tau_b}{\Delta T}\left[1 - \frac{1}{(1+\Delta T)^{1/2}}\right] \tag{37}$$

For $T(\tau_b)$ 40 eV, $T(0) = 4$ eV, $\tau_b = 50$ ns, $V_y/V_z \gtrsim 0.08$ and $n_b/n_p = 10^{-3}$, $\delta \lesssim 1.0$ e-folds. A spread in V_y then reduces the growth of the ion-Whistler instability to a tolerable level.

Finally it can also be shown that the ion-Whistler instability does not convect with the beam when $k_z \gtrsim 0$. This needs to be verified in order to justify using τ_b as the appropriate time scale. Taking Eq. (5) for f_b and setting $k = k_y\hat{e}_y + k_z\hat{e}_z$ this dispersion equation becomes

$$0 = c^2k_y^2 - (\omega_r + i\gamma)^2 + \frac{\omega_{pi}^2}{\nu_i}(\omega_r + i\gamma) + I_{zz}, \tag{38}$$

where $\omega = \omega_r + i\gamma$ and

$$I_{zz} = \frac{\omega_{pb}^2}{2\pi}\int_o^{2\pi} d\phi\left[\frac{\omega^2 + k_y^2(V_z^2 + 2V_zV_\beta\cos\phi + V_\beta^2\cos^2\phi)}{(\omega - k_zV_z - k_zV_\beta\cos\phi)^2}\right] \tag{39}$$

Here the spread in v_y is neglected since it will have little effect on the axial group velocity of the perturbation. For mathematical convenience finite geometry effects and the betatron motion of the beam ions are also ignored. The results of the present calculation is actually an upper limit on the group velocity since the betatron motion of the beam ions will tend to wash out any disturbance moving axially on the beam. For $|\omega_r - k_zV_z| > k_zV_\beta$ the denominator of the integrand in Eq. (39) can be expanded and the integration is trivial. However, if $|\omega_r - k_zV_z| \lesssim k_zV_\beta$ the integration is most easily done using the calculus of residues. For small k_z and $V_\beta < V_z$, $|\omega_r - k_zV_z| > k_zV_\beta$ is appropriate for the ion-Whistler instability. Then integrating Eq. (39), Eq. (38) can be solved for ω_r and γ yielding

$$\gamma = \frac{\omega_{pb}}{c}(V_z^2 + V_\beta^2/2)^{1/2} - k_z V_z, \tag{40}$$

$$\omega_r = \frac{3}{2}\, k_z^2 V_z c/\omega_{pb}. \tag{41}$$

Clearly, $v_g = \partial\omega_r/\partial k_z < V_z$ for $k_z < \omega_{pb}/3c$. Thus the ion-Whistler instability does convect in the axial direction for $k_z < \omega_{pb}/3c$, but with a group velocity slower than the beam streaming velocity. For $k_z > \omega_{pb}/3c$ the calculus of residues can be used to evaluate Eq. (39), however, the mode is then basically an electrostatic two stream mode. This mode has already been shown to be stable in Ref. 1.

In summary it is found that, as expected, the betatron motion of the beam ions does not affect the ion-Whistler instability. The peak growth rate, however, can be reduced to a tolerable level by the presence of a spread in v_y (angular momentum in cylindrical geometry). The spread in v_y known to be present at injection in typical experiments[2] is sufficient to reduce the number of e-folds to less than 1.0. Furthermore, the mode convects axially at a group velocity less than V_z. The electron-Whistler instability was not considered, since it will have properties similar to the properties of the electron-Weibel instability (discussed in Section II.B) for such a highly collisional plasma ($\nu_e > \omega_{ce}$).

V. CONCLUSIONS

The purpose of this paper was to study electromagnetic velocity-space instabilities generated by a focused ion beam propagating through a z-discharge plasma. In particular, the Weibel instability ($\mathbf{k} \cdot \mathbf{B} = 0$, $\mathbf{k} \cdot \mathbf{V}_z \approx 0$) and the Whistler instability ($\mathbf{k} \times \mathbf{B} \approx 0$, $\mathbf{k} \cdot \mathbf{V}_z \approx 0$) were investigated. This work is an extension of the work in Ref. 1, where electrostatic instabilities were investigated.

The ion-Weibel instability (driven by the streaming energy of the beam ions) is found to be stabilized by the betatron motion of the beam ions at the front of the beam. At the tail of

the beam, where beam ions follow straight line orbits, the growth of the ion-Weibel instability is two slow to allow for even one e-fold ($\gamma_p^b \tau_b \approx 0.05$) during the transit of the beam. The electron-Weibel instability (driven by the drifting plasma electrons), on the other hand, grows fastest ($\gamma_p^e \tau_b \approx 4.2$) at the front of the beam where the plasma is relatively cold ($T \simeq 4$ eV). At the tail of the beam, where T rises to about 25-50 eV, $\gamma_p^e \tau_b \approx 1.0$. Although the electron-Weibel instability grows faster than the ion-Weibel instability, it also is not expected to grow to a level which could drastically affect beam propagation. Only 1.6 e-folds will occur during the transit of the beam. It has also been shown for $0 < k_z^2 < 2\omega_{pi}^2/3c^2$, where $\mathbf{k} = k_x\hat{\mathbf{e}}_x + k_z\hat{\mathbf{e}}_z$, that the electron-Weibel instability does convect axially but at a group velocity much less than the beam velocity ($v_g = 3k_z^2c^2V_e/2\omega_{pi}^2 < V_e << V_z$). Thus the appropriate growth period for calculating the number of e-folds is just the beam transit time, τ_b, and growth occurs mostly at the tail of the beam.

Because the plasma is highly collisional ($\nu_e > \omega_{ce}$ at all times), the electron-Whistler instability will have properties similar to those of the electron-Weibel instability. Thus it is also not expected to grow to a level which could drastically affect beam propagation.

The ion-Whistler instability, as expected, is not stabilized by the betatron motion of the beam ions. The peak growth rate, however, can be reduced to a tolerable level by the presence of a spread in v_y (angular momentum in cylindrical geometry). Furthermore, for $k_z < \omega_{pb}/3c$ the mode also convects axially at a group velocity less than V_z($v_g = 3k_zcV_z/\omega_{pb}$). Thus τ_b is again the correct time scale and only 1.0 e-fold are expected to occur during the transit of the beam in typical experiments.

From these results and from the results for electrostatic instabilities in Ref. 1, it can be concluded that it is possible to propagate a focused ion beam, appropriate for a pellet fusion

device, through a z-discharge plasma channel without generating significant growth of microinstabilities.

ACKNOWLEDGMENTS

This work was supported by U. S. Department of Energy.

APPENDIX A

For the magnetic field configuration given in Eq. (1) for $|x| < a$ the beam ion orbit equations were solved in paper I. The resulting ion orbits are given below:

$$x' = x \cos \omega_o \tau + \frac{v_x}{\omega_o} \sin \omega_o \tau, \tag{A1}$$

$$y' = y + v_y \tau \tag{A2}$$

$$z' = z + \left[v_z + \frac{\omega_o^2}{4V_z} \left(\frac{v_x^2}{\omega_o^2} - x^2 \right) \right] \tau + \frac{\omega_o}{8V_z} \left(x^2 - \frac{v_x^2}{\omega_o^2} \right) \sin 2\omega_o \tau - \frac{x v_x}{4V_z} (\cos 2\omega_o \tau - 1), \tag{A3}$$

and

$$v_x' = v_x \cos \omega_o \tau - x\omega_o \sin \omega_o \tau, \tag{A4}$$

$$v_y' = v_y, \tag{A5}$$

$$v_z' = v_z - \frac{\omega_o^2}{4V_z} \left(\frac{v_x^2}{\omega_o^2} - x^2 \right) (\cos 2\omega_o \tau - 1) + \frac{\omega_o x v_x}{2V_z} \sin 2\omega_o \tau, \tag{A6}$$

where ω_o and V_z are the same as defined in Section II.

APPENDIX B

The expression for α_1 and α_2 found in Eq. (19) are

$$\alpha_1 = \frac{1}{N}\left\{v_x J_1(X)\left[\frac{1}{2}\,J_o(Y) + J_2(Y)\right]\right. \tag{B1}$$
$$\left. -x\omega_o J_1(Y)\left[\frac{1}{2}\,J_o(X) + J_2(X)\right]\right\},$$

$$\alpha_2 = \frac{1}{N}\left\{(v_z - V_z)\left[\frac{1}{2}\,J_o(X)\,J_o(Y) + 2\sum_{n=1}^{\infty}(-1)^n J_{2n}(X)\,J_{2n}(Y)\right]\right.$$
$$+ \frac{\omega_o^2}{8V_z}\left[\frac{v_x^2}{\omega_o^2} - x^2\right]\left[J_o(X)\,J_o(Y) - 2J_o(X)\,J_2(Y)\right.$$
$$\left. + 2J_o(Y)\,J_2(X) + 4\sum_{n=1}^{\infty}(-1)^n\left[J_{2n}(X)\,J'_{2n+1}(Y) + \frac{2n+1}{X}\,J_{2n}(Y)\,J'_{2n+1}(X)\right]\right]$$
$$\left. - \frac{\omega_o x v_x}{2V_z}\left[J_1(X)\,J_1(Y) + \sum_{n=1}^{\infty}(-1)^n\left[J_{2n+1}(X)\,J'_{2n-1}(Y) + J_{2n-1}(X)\,J_{2n+1}(Y)\right]\right]\right\}, \tag{B2}$$

where $X = kx$, $Y = kv_x/\omega_o$ and $N = r_b + \sin 2kr_b/2k$.

In order to show that

$$I_1 = \frac{-2\omega_{pb}^2}{n_b}\int_{-r_b}^{r_b} dx \cos k_x \int d^3v\left[\frac{kV_z v_z}{\gamma}\,\frac{\partial f_b}{\partial v_\beta^2}\,\alpha_1\right] = 0, \tag{B3}$$

first write $v_x = v_\beta \sin\phi$ and $v_z = V_z + v_\beta\cos\phi$ and then perform the v_y and ϕ integration yielding

$$I_1 = \frac{-\omega_{pb}^2 k V_z^2}{\gamma N}\int_{-r_b}^{r_b} dx \cos kx \int dv_\beta^2\left\{\frac{\partial\delta(v_\beta^2 - V_\beta^2 + \omega_o^2 x^2)}{\partial v_\beta^2}\right.$$
$$\times\left[v_\beta J_1(X)\left[\frac{1}{2}\,J_{-1/2}(Z) + J_{3/2}(Z)\right]J_{1/2}(Z)\right.$$
$$\left.\left. - x\omega_o J_{1/2}^2(Z)\left[\frac{1}{2}J_o(X) + J_o(X)\right]\right]\right\}. \tag{B4}$$

where $Z = kv_\beta/2\omega_o$. Integrating by parts in v_β to remove the derivative of the delta function and then performing the v_β integration results in

$$I_1 = \frac{\omega_{pb}^2 k V_z^2}{4\gamma N \omega_o} \int_{-kr_b}^{kr_b} dX \cos X \left\{ \frac{J_1(X)}{Z} \left[\frac{1}{2} J_{-1/2}(Z) + J_{3/2}(Z) \right] J_{1/2}(Z) \right.$$
$$+ J_1(X) \left[\frac{1}{2} J'_{-1/2}(Z)\, J_{1/2}(Z) + \frac{1}{2} J_{-1/2}(Z)\, J'_{1/2}(Z) \right.$$
$$\left. + J'_{3/2}(Z)\, J_{1/2}(Z) + J_{3/2}(Z)\, J'_{1/2}(Z) \right]$$
$$\left. - \frac{X}{Z} J'_{1/2}(Z)\, J_{1/2}(Z) \left[\frac{1}{2} J_o(X) + J_2(X) \right] \right\}_{Z=\tilde{Z}(x)}, \tag{B5}$$

where $\tilde{Z}(x) = (kr_b/2)\,(1 - x^2/k^2 r_b^2)^{1/2}$. Since the integrand is an odd function of x, $I_1 = 0$.

The integral

$$I_2 = \frac{-2\omega_{pb}^2}{n_b} \int_{-r_b}^{r_b} dx \cos kx \int d^3v \left[v_z \alpha_2 \frac{\partial f_b}{2 v_\beta} \right] \equiv \omega_{pb}^2 F(kr_b) \tag{B6}$$

is more complicated and the associated term in the dispersion relation does not contribute to instability; hence it will suffice to write I_2 in terms of the function $F(kr_b)$ as defined in (B6).

APPENDIX C

For a warm collisional fluid, the continuity equation and momentum transport equations ($T_e \simeq T_i$ and $\nu_i = m_e\nu_e/m_i$) are

$$\frac{\partial n_\alpha}{\partial t} + \nabla \cdot (n_\alpha \mathbf{v}_\alpha) = 0, \tag{C1}$$

$$\frac{\partial \mathbf{v}_\alpha}{\partial t} + \mathbf{v}_\alpha \cdot \nabla \mathbf{v}_\alpha = \frac{q_\alpha}{m_\alpha}\left(\mathbf{E} + \frac{\mathbf{v}_\alpha \times \mathbf{B}}{c}\right) - \frac{T}{m_\alpha n_\alpha}\nabla n_\alpha - \nu_\alpha(\mathbf{v}_\alpha - \mathbf{v}_\beta), \tag{C2}$$

for $\alpha = i,e$. Linearizing Eqs. (C1) and (C2) for perturbations with exp $i(kx - \omega t)$ dependence and solving for the perturbed current results in

$$\mathbf{j}_e + \mathbf{j}_i = \frac{\omega_{pi}^2}{4\pi}\,\mathbf{I} \cdot \mathbf{E}, \tag{C3}$$

where

$$I_{xx} = \left(1 + \frac{\Omega_1^2}{\Omega_2^2}\right)/\Omega_3, \tag{C4}$$

$$I_{xz} = I_{zx} = -ikV_e\Omega_1/\gamma\Omega_2^2, \tag{C5}$$

$$I_{zz} = \frac{1}{\nu_i} - \frac{k^2V_e^2\Omega_3}{\gamma^2\Omega_2^2}, \tag{C6}$$

where $\omega = i\gamma$, $\Omega_1 = \gamma + k^2u_i^2/\gamma$, $\Omega_2^2 = \gamma\nu_i + k^2u_i^2 + 2\nu_ik^2u_i^2/\gamma + k^4u_i^4/\gamma^2$, and $\Omega_3 = \gamma + \nu_i + k^2u_i^2/\gamma$. In deriving expressions (C4)-(C6) it was assumed that $\gamma < \nu_e$.

Here the electron streaming is driving the instability and $n_e \approx n_i$ (unlike $n_b/n_e \ll 1$), thus the complete dispersion equation,

$$D_{xx}D_{zz} - D_{xz}D_{zx} = 0, \tag{C7}$$

must be used. This results in the following dispersion equation

$$0 = \left[\gamma^2 + \frac{\gamma\omega_{pi}^2}{\Omega_3}\left[1 + \frac{\Omega_1^2}{\Omega_2^2}\right]\right]\left[\gamma^2 + c^2k^2 + \frac{\gamma\omega_{pi}^2}{\nu_i} - \frac{\omega_{pi}^2k^2V_e^2\Omega_3}{\gamma\Omega_2^2}\right] + \frac{\omega_{pi}^4k^2V_e^2\Omega_1^2}{\Omega_2^4}. \tag{C8}$$

In order to study the axial convection of the electron Weibel instability, the dispersion equation must be rederived with $|k_z| \gtrsim 0$. For mathematical convenience thermal effects are ignored ($T = 0$ in Eq. (C2)). In this case, for large k_x, the dispersion equation is

$$0 = \left[c^2k_z^2 - \omega^2 - \frac{i\omega_{pi}^2\omega'}{\nu_i}\right]\left[c^2k_x^2 - \frac{ik_x^2V_e^2\omega_{pi}^2(\omega + i\nu_i)}{\omega\omega'\nu_i}\right] - \left[k_zk_xc^2 + \frac{i\omega_{pi}^2k_xV_e}{\nu_i}\right]\left[k_zk_xc^2 + \frac{i\omega_{pi}^2k_xV_e}{\nu_i}\left[1 - \frac{ik_zV_e\nu_i}{\omega\omega'}\right]\right], \tag{C9}$$

where $\omega' = \omega - k_zV_e$ and now $\omega = \omega_r + i\gamma$.

REFERENCES

1. P. F. Ottinger, D. Mosher and S. A. Goldstein, Phys. Fluids 22, 332 (1979).

2. F. Sandel, G. Cooperstien, S. A. Goldstein, D. Mosher and S. J. Stephanakis, Bull. APS 23, 816 (1978).

3. D. A. Hammer and N. Rostoker, Phys. Fluids 13, 1831 (1970).

4. D. Mosher, D.G. Colombant, S.A. Goldstein and R. Lee, in *IEEE Conference Record-Abstracts, 1978 IEEE International Conference on Plasma Science, Monterey, California* (IEEE, New York, 1978) p. 113.

5. R. Lee and M. Lampe,. Phys. Rev. Lett. 31, 1390 (1973).

6. K. Molvig, Phys. Rev. Lett. 35, 1504 (1975).

7. S. A. Bludman, K. M. Watson and M. N. Rosenbluth, Phys. Fluids 3, 747 (1960).

8. B. D. Fried and S. D. Conte, "The Plasma Dispersion Function" (Academic, New York, 1961).

9. G. Arfken, "Mathematical Methods for Physicists," 2nd ed. (Academic, New York, 1970) p. 474.

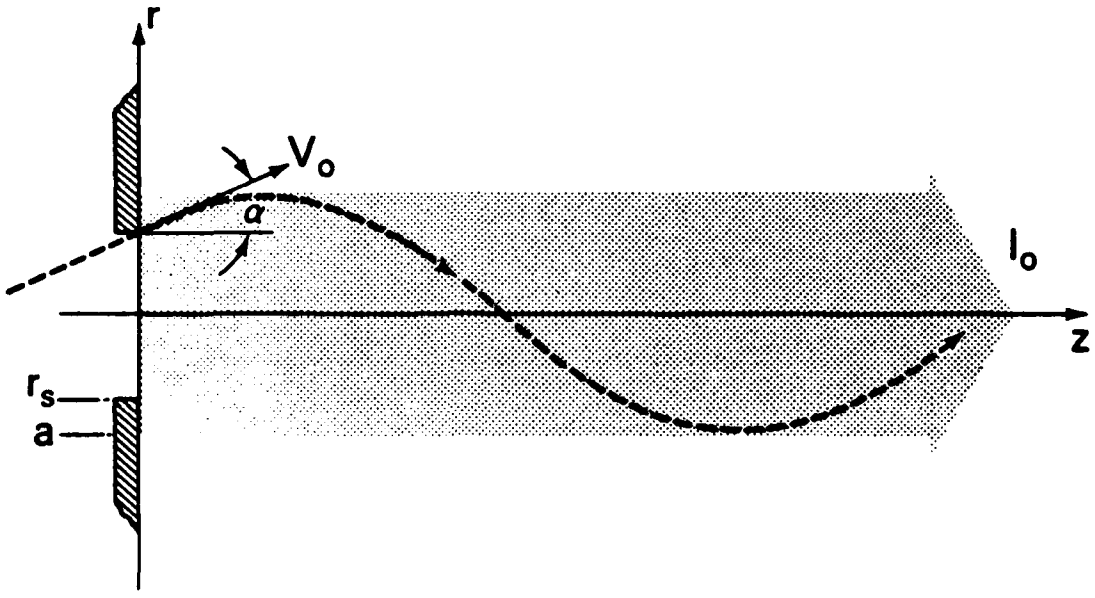

Figure 1 — Typical ion trajectory in the confining azimuthal magnetic field of the z-discharge channel after entering the channel from the focussing region on the left. Here V_0 is the speed of the beam ion, α in the injection angle, r_s is the spot size at injection and a is the channel radius.

APPENDIX 2. Ion Beam Propagation in a Filamented Channel.

ION BEAM PROPAGATION IN A FILAMENTED CHANNEL

I. INTRODUCTION

The production of intense focused ion beams[1] has led to the consideration of using z-discharge plasma channels to transport them several meters to inertial fusion targets[2]. Analysis has shown that although electrostatic beam-plasma streaming modes are stable[3], electromagnetic microinstabilities will occur during transport in such channels[4]. The fastest growing mode produces current bunching of the electrons in the channel. In this report ion beam propagation in a filamented channel is investigated in order to determine the effects on radial beam containment in channels and on the radial beam density profile.

In Sec. II, radial current bunching in the channel is considered and in Sec. III, azimuthal current bunching is considered. Finally the results of this work are summarized in Sec. IV.

II. RADIAL CURRENT BUNCHING IN THE CHANNEL

If $\underline{k} = k\,\hat{e}_r$, then radial current bunching occurs in the channel and the net current density can be modeled by

$$\underline{j} = \left[\bar{j}(r) + j_1\, H(r-r_b)\, J_o(kr)\right] \hat{e}_z \quad , \tag{1}$$

where

$$H(r-r_b) = \begin{cases} 1 \, , & 0 \leq r \leq r_b \\ 0 \, , & r > r_b \end{cases} ,$$

r_b is the beam radius and J_o is the zero order Bessel function which satisfies the wave equation in cylindrical coordinates. For

Note: Manuscript submitted January 2, 1980.

a channel of radius r_c

$$I_o = 2\pi \int_o^{r_c} j(r)\, r dr = 2\pi \int_o^{r_c} \bar{j}(r)\, r dr$$

is the channel current which confines the ion beam. Here $k \equiv a_{1\ell}/r_b$ was used, where $a_{1\ell}$ is the ℓ^{th} zero of first order Bessel function J_1. The second term on the right hand side of Eq. (1) is then the residual current density arising from the bunched electron current superimposed on the unbunched ion beam current. Since $j(r)$ is established in an initially cold plasma and is driven by a capacitor bank on a time scale much longer than the beam pulse duration, when the beam is injected into the now highly conducting plasma the total net current resists change. Thus, in the absence of bunching $\underset{\sim}{j} = \underset{\sim}{j}_e + \underset{\sim}{j}_b = \bar{j}(r)\, \hat{e}_z$, where $\bar{j} \ll j_b$.

The magnetic field which determines the ion motion in a filamented channel is then found from

$$\frac{1}{r} \frac{\partial}{\partial r} (r B_\theta) = \frac{4\pi}{c} \left[\bar{j}(r) + j_1 J_o(kr) \right] \quad , r \le r_b. \tag{2}$$

Assuming $\bar{j}(r) = j_o (r/r_c)^{s-1}$ inside the channel ($s \ge 1$),

$$B_\theta = \frac{4\pi j_o r^s}{(s+1)\, c\, r_c^{s-1}} + \frac{4\pi j_1}{kc} J_1(kr) \quad , \quad r \le r_b, \tag{3}$$

where $r_c > r_b$. The parameter s is a magnetic field shaping factor which is equal to one at the front of the beam and increases as one moves toward the tail of the beam. The beam heated plasma in the channel at the tail of the beam expands radially carrying the channel current with it. This decreases the magnetic field (increases s) near the center of the beam and produces a sharply rising magnetic field at the edge of the

beam.[5]

The total energy H, the axial cononical momentum P_z, and the canonical angular momentum P_θ are all constants of the motion for the ions. From $A_z = -\int B_\theta dr$ and Eq. (3), P_z is found to be

$$\frac{P_z}{m_i} = \dot{z} - \frac{2\omega_{cb} r_c}{(s+1)} \left(\frac{r}{r_c}\right)^{s+1} - \frac{2\omega_{cb}(s+1) j_1}{k^2 r_c j_o} \left[1 - J_o(kr)\right], \qquad (4)$$

where $\omega_{cb} = 2\pi e r_c j_o / m_i c^2 (s+1)$. When $j_1/j_o > 0$, it is clear that the beam ion orbits are radially confined since $1 - J_o(kr) \geq 0$ and r^{s+1} is monotonically increasing. When $j_1/j_o < 0$, the ion orbits are also radially confined if $\left| j_1/j_o \right|$ is sufficiently small since $\left[1 - J_o(kr)\right] \leq \left[1 - J_o(a_{11})\right] \simeq 1.4$ and r^{s+1} is a monotonically increasing function of radius.

Now consider this result in more detail. Since $P_\theta = 0$[6], the minimum axial canonical momentum is given by

$$P_z^o = m_i \left[V_o \cos\alpha_o - \frac{2\omega_{cb} r_c}{(s+1)} \left(\frac{r_s}{r_c}\right)^{s+1} \right], \qquad (5)$$

when $j_1 = 0$. Here α_o is the maximum ion injection angle, $V_o = (2H/m_i)^{1/2}$ and r_s is the beam focal spot size at the point of injection into the channel. The beam envelop radius is then

$$r_b^o = r_c \left[\frac{(s+1)}{2\omega_{cb} r_c} \left(V_o - \frac{P_z^o}{m_i} \right) \right]^{\frac{1}{s+1}} \qquad (6)$$

where $r = r_b^o$ when $\dot{z} = V_o$ for an ion injected with $P_z = P_z^o$. When $s = 1$ the usual result is recovered[6]

$$r_b^o = r_c \left[\frac{V_o}{\omega_{cb} r_c} \left(1 - \frac{P_z^o}{m_i V_o} \right) \right]^{1/2} \qquad (7)$$

When $j_1 \neq 0$, the minimum axial canonical momentum is given by

$$p_z^1 = p_z^o - \frac{2m_i j_1 \omega_{cb}^{(s+1)}}{j_o k^2 r_c} \left[1 - J_o(kr_s)\right], \qquad (8)$$

where this result only strictly applies for $\left|j_1/j_o\right| < kr_c(r_s/r_c)^s/(s+1)$. In this case the beam envelope radius is found from

$$\frac{2}{(s+1)}\left(\frac{r_b}{r_c}\right)^{s+1} + \frac{2j_1(s+1)}{j_o k^2 r_c^2}\left[1-J_o(kr_b)\right] = \frac{V_o}{\omega_{cb} r_c}\left(1-\frac{p_z^1}{m_i V_o}\right). \qquad (9)$$

For $\left|j_1/j_o\right| \ll 1$ this reduces to

$$r_b \approx r_b^o\left(1 - \frac{j_1}{j_o}\frac{(s+1)}{(kr_b^o)^2}\left(\frac{r_c}{r_b^o}\right)^{s-1}\left[2 - J_o(kr_b^o) - J_o(kr_s)\right]\right), \qquad (10)$$

so that for $j_1 < 0$ the beam radius expands, whereas for $j_1 > 0$ the beam radius decreases. For larger $\left|j_1/j_o\right|$ Eq. (9) must be solved numerically.

When $j_1 < 0$, beam ions can be magnetically trapped and prevented from reaching the axis if $\left|j_1/j_o\right|$ is sufficiently large. Thus the density profile could be depressed on axis. For a given ion injected into the channel at a radius r_o and at an injection angle α trapping occurs if

$$\left|\frac{j_1}{j_o}\right| > \frac{k^2 r_c^2}{\left[1-J_o(kr_o)\right]}\left[\frac{V_o(1-\cos\alpha)}{2\omega_{cb} r_c(s+1)} + \frac{(r_o/r_c)^{s+1}}{(s+1)^2}\right]. \qquad (11)$$

When $s = 1$ and $\alpha \ll 1$, this reduces to

$$\left|\frac{j_1}{j_o}\right| > \frac{k^2 r_c^2/4}{\left[1-J_o(kr_o)\right]}\left[\frac{V_o \alpha^2}{2\omega_{cb} r_c} + \left(\frac{r_o}{r_c}\right)^2\right] \geq 1, \qquad (12)$$

so that trapping begins when the bunched current density exceeds the magnitude of the channel current density which is required to confine the beam. Furthermore, Eq. (9) shows that the equilibrium beam radius is

also significantly modified if $\left|j_1/j_o\right| > 1$.

Thus when radial current bunching occurs in the channel, good beam propagation is still expected unless $\left|j_1/j_o\right|$ exceeds unity. If $\left|j_1/j_o\right| > 1$, the beam will be expelled from the center of the channel when $j_1 < 0$ or the beam will pinch when $j_1 > 0$. If r_b becomes larger than r_c the analysis breaks down and a more sophisticated analysis is required, however, it has been established here that it is desirable to maintain $\left|j_1/j_o\right| < 1$. For $j_1 \approx j_n \exp(\gamma \tau_b)$, good beam propagation requires $j_n < j_o \exp(\gamma \tau_b)$. Here γ is the growth rate of the instability, τ_b is the beam pulse duration and j_n is the initial level of noise in the electron current. Since the predominant source of j_n is the nonuniformities in the radial profile of the ion beam current density (remember $j_e = j_b + \bar{j}$), jitter in the ion beam current density must be kept below

$$\frac{j_{bn}}{j_b} < \frac{j_o}{j_b} \exp(-\gamma \tau_b). \tag{13}$$

Typically $\gamma \tau_b \sim 1.0 - 2.0$ and $j_o/j_b \sim 0.1$ for proposed fusion systems.[4] Thus the jitter in the beam current density must be kept below 1 - 4%. Since the filamentation instability is nonconvective[4], these results only apply at the tail of the beam. At the front of the beam the limit on j_{bn}/j_b stated in Eq. (13) is less severe and can be found by replacing $\gamma \tau_b$ by $\gamma \tau_b x/x_b$ where x is the distance from the front of the beam for a beam of length x_b.

III. AZIMUTHAL CURRENT BUNCHING IN THE CHANNEL

If $\underset{\sim}{k} = k\hat{e}_\theta$ then azimuthal current bunching occurs in the channel and the net current density can be modeled by

$$\underset{\sim}{j} = (\bar{j}(r) + j_1 H(r-r_b)\sin m\theta)\hat{e}_z \ , \tag{14}$$

where $m = 3,4,5,\ldots$ will be considered. Special treatment is required for $m = 1,2$ which is not considered here since $m \approx 3$-7 in typical cases.[4] Again

$$I_o = \int j(r,\theta)\, r dr = 2\pi \int \bar{j}(r) r\, dr$$

is the channel current which confines the ion beam and $j_1 \sin m\theta$ is the residual current density arising from the bunched electron current superimposed on the unbunched ion beam current. The magnetic field which determines the ion motion in a filamented channel is then

$$B_\theta = \frac{4\pi j_o r^s}{(s+1)c r_c^{s-1}} - \frac{8\pi j_1 r}{c(m^2-4)} \sin m\theta \ , \ r \le r_b, \tag{15}$$

$$B_r = \frac{4\pi j_1 r}{c(m^2-4)} \cos m\theta \ , \quad r \le r_b \tag{16}$$

where again $\bar{j}(r) = j_o(r/r_c)^{s-1}$ was assumed.

In this case H and P_z are constants of the motion but P_θ is not. From Eq. (15) P_z is found to be

$$\frac{P_z}{m_i} = \dot{z} - \frac{2\omega_{cb} r_c}{(s+1)^2}\left(\frac{r}{r_c}\right)^{s+1} + \frac{2\omega_{cb} r^2 j_1 \sin m\theta}{r_c(m^2-4)j_o} \ , \ r \le r_b. \tag{17}$$

Solving Eq. (17) for $\dot{z}$ shows that as long as

$$\left|\frac{j_1}{j_o}\right| \le \frac{m^2-4}{(s+1)^2} \ , \tag{18}$$

where $r_c \ge r_b$, all ion orbits are confined within the channel. For larger $|j_1/j_o|$ ions can escape from the channel and the beam density is

gradually depleted.

Even for small $|j_1/j_o|$ the beam density on axis decreases in time since $|P_\theta|$ increases in time for most ions. In fact P_θ is constant only for those few ions which are injected at $\theta_o = n\pi/m$ (n = 1,2,3,...,2m). For $|j_1/j_o| \ll 1$

$$(R^2\theta')' = -R(R'' - R\theta'^2)\left(\frac{2mj_1 \cos m\theta}{j_o(m^2-4)}\right) , \tag{19}$$

where $R = Kr$, $\tau = \Omega t$, $K^2 = m_i\omega_{cb}/P_z r_c$, $\Omega^2 = P_z\omega_{cb}/m_i r_c$ and a prime signifies differentiation with respect to τ. Thus, to zero order in the small parameter $|j_1/j_o|$

$$(R^2\theta')_o = K^2P_\theta/\Omega = \text{const.} \tag{20}$$

If P_θ is initially zero and $R_o \approx A\cos(\tau + \varphi)$ (implying small injection angles,[6] i.e. $\alpha \ll 1$) the time averaged increase in $|P_\theta|$ can be expressed as

$$\frac{\langle|P_\theta|\rangle}{r_o V_o \alpha} = t/\tau , \tag{21}$$

where $r_o V_o \alpha \approx r(z=o)\dot{r}(z=o)$ and

$$\tau = \frac{r_o\alpha(m^2-4)|j_o/j_1|}{mV_o \cos m\theta_o}\left(\alpha^2 + \frac{r_o^2\omega_{cb}}{V_o r_c}\right)^{-1} . \tag{22}$$

Thus in a time τ, $|P_\theta|$ increases from zero to $r_o V_o \alpha$. For the average ion $\langle|\cos m\theta_o|\rangle = 2/\pi$, $r_o \approx r_b/2$, $\alpha \approx \alpha_o/2$ and

$$\bar{\tau} = \frac{\pi r_b\alpha_o(m^2-4)|j_o/j_1|}{2mV_o}\left(\alpha_o^2 + \frac{r_b^2\omega_{cb}}{V_o r_c}\right)^{-1} . \tag{23}$$

Typically $r_b \approx 0.4$ cm, $\alpha_o \approx 0.2$ rad, $m \approx 5$, $V_o \approx 3.1 \times 10^9$ cm/sec and $\omega_{cb} \approx 4 \times 10^8$ sec^{-1} so that

$$\bar{\tau} \approx 2.3 \times 10^{-9} \left| j_o/j_1 \right| \text{ sec.} \tag{24}$$

Thus the beam hollows out on a time scale of $\bar{\tau}$ even for small $\left| j_1/j_o \right|$, although the beam is still confined within the channel. In order to prevent this hollowing out from occurring during beam propagation one needs $\tau_t < \bar{\tau}$ or

$$j_n < \frac{\pi r_b \alpha_o (m^2-4) j_o}{2mL} \left(\alpha_o^2 + \frac{r_b^2 \omega_{cb}}{V_o r_c} \right)^{-1} \exp(-\gamma \tau_b) \ , \tag{25}$$

where $\tau_b = L/V_o$ is the beam transit time in a channel of length L and again j_n is the initial noise level in the electron current. Thus as argued at the end of Sec. II this implies that the jitter in the ion beam current density must be kept below

$$\frac{j_{bn}}{j_b} < \frac{\pi r_b \alpha_o (m^2-4)}{2mL} \frac{j_o}{j_b} \left(\alpha_o^2 + \frac{r_b^2 \omega_{cb}}{V_o r_c} \right)^{-1} \exp(-\gamma \tau_b) \ . \tag{26}$$

Typically this is found to be $j_{bn}/j_b \sim 1 - 5 \times 10^{-4}$ for proposed fusion systems. Since this low level of noise is probably not achievable, some hollowing out of the beam is likely if current bunching occurs, however the beam will still be confined in the channel for small $\left| j_1/j_o \right|$. This effect will be most pronounced at the tail of the beam where largest growth of the nonconvective filamentation instability occurs.[4]

For $\left| j_1/j_o \right| \geq (m^2-4)/(s+1)^2$ the beam density is gradually depleted as increasingly more ions become unconfined. This depletion will occur in addition to the hollowing out of the beam and also occurs predominately at the tail of beam. In order to prevent this beam density depletion

one needs

$$\frac{j_{bn}}{j_b} < \frac{(m^2-4)}{(s+1)^2} \frac{j_o}{j_b} \exp(-\gamma\tau_b) \qquad (27)$$

For $m \sim 5$, $s \sim 4$, $j_o/j_b \sim 0.1$ and $\gamma\tau_b \sim 1 - 2$ at the tail of the beam, $j_{bn}/j_b \lesssim 1 - 4\%$ is required. At the front of the beam the condition is much less severe with $\gamma\tau_b$ replaced by $\gamma\tau_b x/x_b$ where x is the distance from the front of the beam for a beam of length x_b. Eq. (26) can be similarly modified for the front portion of the beam.

IV. CONCLUSIONS

From the analysis presented here it can be concluded that good beam transport in a filamented z-discharge channel is possible as long as the current bunching remains below certain levels. For radial current bunching it was found that $|j_1/j_o|$ should not exceed unity, which implies that $j_n < j_o \exp(-\gamma\tau_b)$. If $|j_1/j_o|$ exceeds unity, the beam will be expelled from the center of the channel when $j_1 < 0$ or the beam will pinch when $j_1 > 0$.

For aximuthal current bunching the beam hollows out on a time scale $\bar{\tau}$ defined in Eq. (23). This hollowing out occurs for all values of $|j_1/j_o|$ but will not reach a significant level if $\tau_t < \bar{\tau}$ (see Eq. (25). For $|j_1/j_o| \geq \frac{m^2-4}{(s+1)^2}$ the beam density is also gradually depleted as increasingly more ions become unconfined.

These results set limits on the level of j_{bn} which can be tolerated without seriously affecting beam transport due to current bunching effects.

V. REFERENCES

1. S. J. Stephanakis, G. Cooperstein, Shyke A. Goldstein, D. Mosher, F. W. Oliphant, F. L. Sandel and F. C. Young, in IEEE Conference Record-Abstracts, 1979 IEEE International Conference on Plasma Science, Montreal, Quebec, Canada (IEEE, New York, 1979) p.79.
2. Shyke A. Goldstein, D. Mosher, P. F. Ottinger and W. W. Hsing, in Inertial Confinement Fusion (Optical Society of America, San Diego, CA, 1978) p. WB7-1.
3. P. F. Ottinger, D. Mosher and Shyke A. Goldstein, Phys. Fluids 22, 332 (1979).
4. P. F. Ottinger, D. Mosher and Shyke A. Goldstein Bull. Am. Phys. Soc. 23, 800 (1978); manuscript submitted to Phys. Fluids.
5. D. G. Colombant, Shyke A. Goldstein and D. Mosher, in IEEE Conference Record-Abstracts, 1979 IEEE International Conference on Plasma Science, Montreal, Quebec, Canada (IEEE, New York, 1979) p. 105.
6. P. F. Ottinger, D. Mosher and Shyke A. Goldstein, in IEEE Conference Record-Abstracts, 1979 IEEE International Conference on Plasma Science, Montreal, Quebec, Canada (IEEE, New York, 1979) p. 105.

APPENDIX 3. Propagation of Intense Ion Beams in Straight and Tapered Z-Discharge Plasma Channels.

PROPAGATION OF INTENSE ION BEAMS IN STRAIGHT AND TAPERED Z-DISCHARGE PLASMA CHANNELS

P. F. Ottinger, [a] D. Mosher, and Shyke A. Goldstein[a]
Naval Research Laboratory,
Washington, D. C. 20375

ABSTRACT

A preformed z-discharge plasma channel can be used to transport focused ion beams appropriate for a pellet-fusion device. During transport, the beam can be compressed axially by time-of-flight bunching when appropriate ion accelerating voltage waveforms are employed. Single-particle orbits in such channels are expressible in terms of simple harmonic functions for small ion injection angles. In this work, orbit analysis is used to investigate how non-uniformities or tapering of the channel and electric fields present in the channel effect radial beam confinement and power multiplication by bunching.

a) Present address: JAYCOR, Alexandria, Virginia 22304

I. INTRODUCTION

In order to utilize intense light ion beams (e.g., 2-10 MeV protons or deuterons) in a pellet fusion device, it is generally considered necessary to propagate the beam a distance of 2-10 m from the acceleration region while employing some focusing scheme to deliver the beam to the target. One concept[1] involves concentrating the beam by one order-of-magnitude in radius at a point 20-50 cm in front of a small-area ion diode by a combination of geometric and self-magnetic-field focusing techniques.[2] At the focus, the beam enters a z-discharge plasma channel which guides it to the vicinity of the pellet. The beam is confined to the discharge channel during propagation by the azimuthal magnetic field produced by the current driving the discharge and is delivered on target with no additional focusing. Figure 1 illustrates trajectories of typical ions in such a system.

Since good propagation requires conditions in the channel to provide nearly complete beam charge and current neutralization,[3] the beam ions do not experience collective effects. Single particle orbits are determined primarily from the equations of motion for a beam ion in the channel azimuthal magnetic field. When the ion injection angle into the channel is small, these betatron orbits can be expressed in terms of simple harmonic functions as demonstrated in Sec. II.

Using the results of Sec. II, the z-dependence of the radial beam density profile is obtained in Sec. III by following the single particle orbits of an ensemble of beam ions injected into the channel. Both analytical and numerical results are presented for rippling of the beam envelope.

The possibility of using axial bunching and radial compression of the beam to achieve beam power multiplication[4] has led to a study of ion orbits in a tapered z-discharge channel. In Sec. IV, the method of multiple scales[5] is used to find the dependence of the beam envelope radius on the axial position in a tapered channel. The limits on power-density multiplication due to axial velocity dispersion in tapered channels is also determined.

The effects on the ion orbits of small axial and radial electric fields induced by beam passage through the channel are investigated in Secs. V and VI respectively. These analyses determine the range of field strengths which permit good beam propagation without significant radial expansion or slowing down of the beam.

If the plasma channel is subject to magnetohydrodynamical instabilities, beam propagation may be affected. In Sec. VII this problem is studied using a code which solves the equations of motion for an ion injected into a bumpy channel. The amplitude of the bump was randomly varied in order to more closely simulate the nonlinear evolution of sausage instabilities. Analytical results in the form of a Mathieu equation are presented which determine the importance of particle resonances in a constant-amplitude bumpy channel. The focusing and stability properties of ion orbits in these channels are also investigated.

Finally in Sec. VIII, the results of this work are summarized and some concluding remarks are made.

The z-discharge plasma channel providing radial confinement for the focused ion beam may be formed microseconds before beam injection so that complete magnetic diffusion occurs. The high plasma density of the channel ($n_p \approx 10^{18}$ cm^{-3}) insures good charge neutralization of the beam.[3] Good beam current neutralization in the interior of the beam also occurs because of the rapid increase in the conductivity due to beam heating.[3,6] Thus, the total magnetic field is comparable to that associated with the performed channel established before injection. The net current, which is approximately given by the channel current, is about an order of magnitude less than the bare beam current.

Modeling the channel current by a uniform current profile, the azimuthal magnetic field is given by

$$B_\theta = \begin{cases} B_o r/r_c, & r<r_c \\ B_o r_c/r, & r>r_c \end{cases} , \qquad (1)$$

where r_c is the radius of the current channel. In a carefully-mounted experiment, imperfect focusing is due primarily to ion-orbit deviations produced by such time-varying, azimuthally symmetric electromagnetic fields in the diode. These fields displace the ions away from the geometric point focus. At the best-focus location, ions produced on opposite sides of the diode merge into the same spatial region creating a spread in angles of ions entering the transport region. These diode fields do not impart azimuthal velocity to the ions so that the angular spread in injection velocities lies primarily in the r-z plane rather than a cone. Since the experimental techniques[2] used to focus the beam are not expected to produce large azimuthal asymmetries in the diode fields, angular momentum effects can be ignored in the lowest-order ion motion. Modifications of the results presented here due to azimuthal motion are presently under investigation. Some numerical results are presented in Secs. III and VII.

The equations of motion for an ion confined within such a channel (i.e., $r<r_c$) are just

$$\ddot{r} = -\omega_{cb}\dot{z}r/r_c \quad , \tag{2}$$

$$\dot{z} = \omega_{cb}\dot{r}r/r_c \quad , \tag{3}$$

where $\omega_{cb} = eB_o/m_i c$. Although it has been shown[7] that the general solutions of these equations can be written in terms of elliptic functions, simple solutions corresponding to the $\dot{r}/\dot{z} << 1$ case at hand are derived. These analytic forms provide a basis for calculations to follow.

Normalizing Eqs. (2) and (3)

$$R'' = -Z'R \quad , \tag{4}$$

$$Z'' = R'R \tag{5}$$

where $R = Kr$, $Z = Kz$, $\tau = \Omega t$, $K^2 = \omega_{cb}/r_c V_o \cos\alpha_o$, $\Omega^2 = \omega_{cb} V_o \cos\alpha_o/r_c$, V_o = const is the speed of the ion, α_o is the angle of injection into the channel and a primed quantity signifies $d/d\tau$. Here K is the betatron wavenumber and Ω is the betatron frequency of the beam ion.

If the ion enters the channel at a small angle to the axis, then the small magnetic field required to confine the ions results in $\epsilon = Kr_c << 1$, and a simple expansion technique can be used to solve Eqs. (4) and (5). Details of this technique can be found in Ref. 5. Writing

$$R = \epsilon R_1 + \epsilon^2 R_2 + \ldots \quad , \tag{6}$$

$$Z = Z_o + \epsilon Z_1 + \epsilon^2 Z_2 + \ldots \quad , \tag{7}$$

$$\eta = (1 + \epsilon\omega_1 + \epsilon^2 \omega_2 + \ldots)\tau \quad , \tag{8}$$

and collecting terms of like powers in ϵ, leads to a set of equations which can be solved to any desired order in the small parameter ϵ. In solving these equations, care must be taken to remove secular terms. The solution of Eqs. (2) and (3) is then

$$z = \left(V_o \cos\alpha_o - \frac{\omega_{cb}\bar{r}^2}{4 r_c} \cos 2\phi\right)t \qquad (9)$$

$$+ \frac{\bar{r}^2}{8r_c} \left(\frac{r_c\omega_{cb}}{V_o \cos\alpha_o}\right)^{\frac{1}{2}} \left[\sin 2 (\omega_\beta t + \phi) - \sin 2\phi\right] + O(\varepsilon^3),$$

$$r = \bar{r} \cos (\omega_\beta t + \phi) + O(\varepsilon^3), \qquad (10)$$

where

$$\omega_\beta = \Omega \left(1 - \frac{\omega_{cb}\bar{r}^2}{16 r_c V_o \cos\alpha_o} + \frac{\tan^2\alpha_o}{4}\right) ,$$

$$\tan\phi = -\left(\frac{r_c V_o \cos\alpha_o}{\omega_{cb} r_o^2}\right)^{\frac{1}{2}} \tan\alpha_o ,$$

$$\bar{r} = \left(r_o^2 + \frac{r_c V_o \sin^2\alpha_o}{\omega_{cb} \cos\alpha_o}\right)^{\frac{1}{2}} ,$$

and $r(0) = r_o$, $z(0) = 0$, $\dot{r}(0) = V_o \sin\alpha_o$ and $\dot{z}(0) = V_o \cos\alpha_o$.

The maximum angle of injection, α_m, in typical experiments and for proposed fusion systems[4] is on the order of 0.1-0.2 radians. Since the ions should be confined within the channel ($r \leq r_c$), Eq. (10) requires that

$$I_o(A) \geq (1.57 \times 10^7 \mu\alpha_m^2 V_o/c) (1 - r_s^2/r_c^2)^{-1} , \qquad (11)$$

where I_o is the channel current, μ is the ratio of the beam ion mass to the proton mass, and r_s is the beam spot size at injection into the channel. This same result can be obtained directly from the conservation of axial

canonical momentum which states that

$$\dot{z} = V_o \cos\alpha_o + (eI_o/m_i r_c^2 c^2)\,(r^2 - r_o^2) \quad . \tag{12}$$

Equation (11) is recovered when $\dot{z} = V_o$, $\alpha_o = \alpha_m$, $r = r_c$ and $r_o = r_s$ (also $1 - \cos\alpha_m \approx \alpha_m^2/2$). For a 5 MeV proton beam with $\alpha_m = 0.2$ radians, $r_s = 0.4$ cm and $r_c = 0.6$ cm, Eq. (11) states that $I_o \geq 113.0$ kA.

Equation (9) shows that the z-motion has both a streaming component and an oscillatory part and that an ion transit time in the channel can be expressed as

$$\tau_t = z_t/V_o + O(\varepsilon^2) \quad , \tag{13}$$

where z_t is the channel length. The $O(\varepsilon^2)$ corrections to τ_t are important when axial bunching is considered,[4] since different ions injected into the channel at the same time will arrive at the target at different times. The spread in arrival times for a straight channel,

$$(\Delta t_a)_s = (z_t/4\,V_o)\,(\alpha_m^2 + \omega_{cb}\, r_s^2/V_o r_c) \quad , \tag{14}$$

can be obtained from time averaging Eq. (12) over the betatron oscillations, and sets a fundamental limit on axial bunching. However, at the point of injection the beam pulse duration, τ_b, is still typically much longer than (Δt_a), thus allowing for considerable axial compression of the beam by proper shaping of the accelerating voltage waveform.

III. BEAM RIPPLING

If the radius of the beam envelope varies with position along the axis of the beam, the beam is said to ripple. In order to obtain good radial confinement of the beam and prevent dramatic increases in beam density at minima of the rippled beam radius, beam rippling should be kept to a minimum. This phenomena arises from coherent oscillatory motion of beam particles injected into a drift region permeated by a confining magnetic field. Although beam rippling occurs in many situations, the coherence length, z_m, can vary widely, making the observation of rippling impossible in some instances ($z_m \leq \lambda_r$, where λ_r is the ripple wavelength). Coherence is lost by phase mising, which for the situation considered is due to the dependence of the betatron frequency on the injection angle of the individual ions. Ions enter the channel at small angles which vary uniformly from α_m to $-\alpha_m$, where α_m is determined by the focusing technique. Since the beam is focused at the entrance to the channel and the focal spot is defined as the point where only random motions determine the beam radius, the distribution of injection angles is independent of injection radius.

Recall from Eq. (10) that the betatron frequency is given by

$$\omega_\beta = (\omega_{cb} V_o/r_c)^{\frac{1}{2}} (1 - \omega_{cb} r_o^2/16 r_c V_o - \alpha_o^2/16) \quad , \qquad (15)$$

where the analysis has been restricted to small injection angles ($\alpha_o \ll 1$). For a collection of ions injected into the channel at z = 0, the betatron frequency varies slightly according to the square of the injection angle and injection radius. The coherence length of the beam ripple can then be determined by following the single particle orbits of a collection of ions.

First Eq. (10) is rewritten as

$$r(t) = r_o \cos \omega_\beta t + (V_o \alpha_o / \bar{\omega}_\beta) \sin \omega_\beta t \quad , \tag{16}$$

where r(t) is the radial position of a given ion at time t and $\bar{\omega}_\beta = (\omega_{cb} V_o / r_c)^{\frac{1}{2}}$. The radial velocity is just

$$v_r(t) = -r_o \bar{\omega}_\beta \sin \omega_\beta t + V_o \alpha_o \cos \omega_\beta t \ . \tag{17}$$

Note that again the small injection angle limit is taken and that $r(0) = r_o$ and $v_r(0) = V_o \sin \alpha_o \simeq V_o \alpha_o$ (also $v_r(t) \approx V_o \alpha(t)$). Also $v_\theta(0) = v_{\theta o}$.

A model for the experimental distribution function is given by

$$f_b(r_o, v_{\theta o}, V_o, \alpha_o) = \begin{cases} N \delta(v_{\theta o}) \delta(V_o - \bar{V}_o) \left| H(\alpha_o + \alpha_m) - H(\alpha_o - \alpha_m) \right|, & |r_o| < r_s \\ 0 \quad , & |r_o| > r_s \end{cases} \tag{18}$$

at z=0 which neglects any small dispersion in $v_{\theta o}$ and approximates the distribution in v_r by a square distribution. Here H is the unit step function

$$H(x - x_o) = \begin{cases} 0 \ , & x < x_o \\ 1 \ , & x > x_o \end{cases} \quad , \tag{19}$$

α_m is the maximum injection angle, r_s is the beam spot size and $m_i \bar{V}_o^2 / 2$ equals the accelerating voltage. The beam density profile at z=0 is found by integrating f_b over velocity space yielding

$$n_b(r_o, 0) = \begin{cases} \bar{n}_b \ , & |r_o| < r_s \\ 0 \ , & |r_o| > r_s \end{cases} \tag{20}$$

where $\bar{n}_b = 2\alpha_m \bar{V}_o N$ is the beam density on axis and r_s is the beam spot size or beam radius at z=0. With injection into the channel at z=0, the beam can be propagated forward by using expressions for r_o and $V_o \alpha_o$ found from Eqs. (16) and (17),

$$r_o = r \cos \omega_\beta t - (v_r / \bar{\omega}_\beta) \sin \omega_\beta t \quad , \tag{21}$$

and

$$V_o \alpha_o = \omega_\beta r \sin \omega_\beta t + v_r \cos \omega_\beta t \quad . \tag{22}$$

Using Eq. (10) to relate z with t,

$$\omega_\beta t \approx \left(\frac{\omega_{cb}}{\bar{V}_o r_c}\right)^{1/2} \left(1 + \frac{3\omega_{cb} r^2}{16 r_c \bar{V}_o} + \frac{3\alpha^2}{16}\right) z \equiv kz \quad , \tag{23}$$

where again r_o and α_o have been written in terms of r and α. The distribution function at a distance z downstream from the point of injection is then

$$f_b(r,z,v_\theta,V,\alpha) = N\left|H\left(\frac{\omega_\beta r}{V}\sin kz + \frac{v_r}{V}\cos kz + \alpha_m\right) - H\left(\frac{\omega_\beta r}{V}\sin kz + \frac{v_r}{V}\cos kz - \alpha_m\right)\right| \times$$
$$\delta\left[|r|\, v_\theta / |r\cos kz - (v_r/\bar{\omega}_\beta)\sin kz|\right] \delta(V-\bar{V}_o), \tag{24}$$

for $|r\cos kz - (v_r/\omega_\beta)\sin kz| \leq r_s$. Here $V=V_o$ and $v_\theta|r| = v_{\theta o}|r_o|$ are constants of the motion.

Equation (23) shows that the dependence on α of the harmonic functions in Eq. (24) is ignorable unless $3\bar{k}\alpha^2 z/16 \gtrsim \pi/4$, which determines the phase mixing distance, z_m. Here $\bar{k} \equiv (\omega_{cb}/r_c V_o)^{1/2}$.

Integrating Eq. (24) over velocity space in order to solve for the beam density profile at z yields $n_b(r,z)$ for $z \ll z_m = 4\pi/3\bar{k}\alpha_m^2$, where $n_b(r,z)$ is given in Eqs. (A1) - (A3) of the Appendix.

For $z \gg z_m$, kz [see Eq. (23)] varies significantly over the range of integration for α in performing the velocity space integration of Eq. (24). Thus, the coherent rippling of the beam is phase mixed out and the beam

density profile becomes independent of z with $n_b(r,z)$ now given by Eq. (A4) of the Appendix. The beam envelope or the outermost radial edge of the beam is given by

$$r_b(z) = \begin{cases} r_s \left| \cos(\pi z/\lambda_r) \right| + (\bar{V}_o \alpha_m/\bar{\omega}_\beta) \left| \sin(\pi z/\lambda_r) \right| , & z << z_m \\ \bar{r}_b , & z >> z_m \end{cases} . \qquad (25)$$

where the phase mixed beam envelope is $\bar{r}_b = (r_s^2 + \bar{V}_o^2 \alpha_m^2/\bar{\omega}_\beta^2)^{1/2}$. From Eq. (25) one finds that the beam does not neck down to a radius smaller than r_s if

$$\bar{V}_o \alpha_m/\bar{\omega}_\beta r_s \geq 1 \qquad (26)$$

Eq. (26) can also be written as a lower limit on I_o given by I_o given by

$$I_o(A) \leq (1.57 \times 10^7 \mu \alpha_m^2 V_o/C)(r_c^2/r_s^2). \qquad (27)$$

Since it is desirable to avoid such necking down to small radii, a good quality beam will satisfy Eq. (27) as well as Eq. (11). Figure 2 illustrates the rippling of a typical beam and Fig. 3 shows the dependence of the coherence length on the maximum injection angle. From Eq. (25) one also finds that the ripple wavelength is given by $\lambda_r \equiv \pi/\bar{k}$.

Although the distribution function (Eq.18) used in this analysis only approximates the actual experimental distribution, the ripple wavelength and coherence length should not depend strongly on the detailed shape of the

distribution function. Provided phase mixing does not depend sensitively on the tail of the α distribution, it should still be possible to obtain a reasonable estimate of the coherence length from Fig. 3 for most distribution functions. Of course, this is only true in the absence of any significant scattering of the beam ions (e.g., due to collisions or "bumpiness" in the channel) or any other mechanism which could significantly enhance phase mixing in the beam (e.g., diode voltage ramping for bunching or nonuniform net current profiles). The ripple amplitude on the other hand, may depend on the details of the distribution function.

In order to obtain numerical results an ensemble of one hundred particles was injected into a channel at $z = 0$. Particles were injected from ten different radii ranging from 0 to r_s and from ten equally spaced injection angles ranging from $-\alpha_m$ to $+\alpha_m$. Because of the cylindrical geometry proportionately more particles were injected at larger radii. The particles were propagated forward in the r-z plane along their trajectories by integrating the equations of motion using a Runge-Kutta routine and eventually collected in radial bins at the desired distance downstream.

The results of this simulation are shown in Figs. 4 and 5, which illustrate the rippling of a beam which is injected into a channel with a distribution function at $z = 0$ given by Eq. (18). Figure 4 clearly shows the beam rippling when

$z << z_m$. For comparison with analytical results the beam density profile at $z = o$ and $z = \lambda_r/2$ are shown in the upper right hand corner. The numerical results at $z = 44.5$ cm and 51.5 cm should be compared with the analytic results at $z = \lambda_r/2$ and the numerical results at $z = 41.0$ cm and 48.0 cm should be compared with the analytic results at $z = o$. The complete analytic form of $n_b(r,z)$ for the injected distribution function given in Eq. (18) is rather complicated and is presented in the Appendix. The good agreement between numerical and analytic results indicate the proper functioning of the code. When $z > z_m$ the coherent rippling of the beam is almost completely lost as illustrated in Fig. 5. Again for comparison with analytic theory an approximate phase mixed density profile is shown in the upper right hand corner of Fig. 5. This profile is obtained from the results presented in the Appendix. The distribution function in Eq. (18) was chosen since it closely resembles the experimental situation. For the proposed parameters used in Figures 4 and 5, the ripple wavelength is $\lambda_r \approx 7.0$ cm and the coherence length is $z_m = 4\pi/3\bar{k}\alpha_m^2 = 230$ cm.

Thus far only motion in the r-z plane has been considered since it has been argued that most of the velocity transverse to the channel axis is in the radial direction. In order to verify that azimuthal motion does not drastically modify the results, the extreme case was also considered where ions are injected into the channel with equivalent spreads in v_r and v_θ. Numerical simulations show results that are similar to those presented in Figs. 4 and 5, however, the addition of angular momentum somewhat reduces the density peak on axis. Beam rippling still occurs for $z < z_m$ and is phase mixed out when $z > z_m$, where z_m is still given by $4\pi/3\bar{k}\,\alpha_m^2$.

If the net current profile is not uniform so that the azimuthal magnetic field does not rise linearly with radius, then the phase mixing distance can be considerably reduced. For $B_\theta \sim r^2$, numerical simulations show that coherence is lost after only a few ripples or about 0.5 m for a typical 5 MeV proton beam with $\alpha_m = 0.2$ rad. This enhanced phase mixing is illustrated in Fig. 6. Such a magnetic field profile could arise if beam injection occurs before magnetic diffusion into the z-discharge channel is completed. Enhanced phase mixing might also occur at the tail of the beam as the now highly conducting plasma (and frozen-in field lines) expands due to beam heating of the channel.

The results of this analysis show that it is possible for ion beams to exhibit coherent rippling over distances of a few meters before phase mixing occurs provided the azimuthal magnetic field rises linearly with radius. Since both the beam radius and density on axis vary with z, beam rippling should be an important consideration when choosing such things as channel parameters ($n_p >> n_b$, $r_c > r_b$, etc.) and target position. The channel current, I_o, and the channel radius, r_c, should be chosen large enough so that the outermost edge of the rippled beam should remain in the channel in order to obtain good radial confinement of the beam. On the other hand, I_o should not be so large that the beam density increases dramatically at minima of the rippled beam radius. Such an occurrence could lead to local heating and microturbulence.[8] Thus, the beam should be matched with the channel (Eq. 27) as well as possible.

IV. BEAM ION ORBITS IN A TAPERED CHANNEL

Although the average beam density on axis may increase by more than a factor of two over the injected beam density on axis after the rippling of the beam has phase mixed out (see Fig. 5), other effects can cause the beam to spread in radius and decrease the beam density on axis (e.g., see Sec. VII). In this section ion orbits in a tapered channel will be determined in order to ascertain the limits of using radial compression of the beam to increase the power density delivered at the target.

If the channel radius decreases linearly such that $r_c(z) = r_c(1-z/L)$, then

$$B_\theta = \frac{2I_o r}{cr_c^2 (1 - z/L)^2} \quad , \quad r < r_c (1 - z/L), \tag{28}$$

where L is the taper length, r_c is the channel radius at z = 0 and Eq. (28) only applies for $(L-z)^2 >> r^2$. Here it is assumed that the beam does not burn its own channel. The equations of motion for an ion confined within this channel are then

$$\ddot{r} = \frac{-\omega_{cb} \dot{z} r}{r_c(1 - z/L)^2} \quad , \tag{29}$$

$$\ddot{z} = \frac{\omega_{cb} \dot{r} r}{r_c (1 - z/L)^2} \quad , \tag{30}$$

where $\omega_{cb} = 2 eI_o/m_i c^2 r_c$. Changing to normalized variables, Eqs. (29) and (30) become

$$R'' = -Z' R/(1 - Z/KL)^2 \tag{31}$$

$$Z'' = R' R/(1 - Z/KL)^2 \quad , \tag{32}$$

where the normalization is the same as in Eqs. (4) and (5). If $\epsilon \equiv Kr_s \ll 1$, then R and Z can be expanded as in Eqs. (6) and (7).

Expanding Eqs. (31) and (32) and collecting terms of equal order in ϵ^m yields to lowest order

$$Z_0'' = 0 \quad , \tag{33}$$

$$R_1'' = -Z_0' R_1/(1 - Z_0/KL)^2 \quad , \tag{34}$$

where it is assumed that $(1 - Z_0/KL) \lesssim O(1)$ (i.e., the ion is not too close to the end of the channel at z = L).

The solution to Eqs. (33) and (34) in terms of the real variables is

$$z(t) = V_0 t + O(\epsilon^2) \quad , \tag{35}$$

$$r(t) = r_0(1 - t/T)^{\frac{1}{2}} \cos \left[-\Omega T \ell n\ (1 - t/T)\right] \tag{36}$$

$$+ (V_0 \sin \alpha/\Omega)\ (1 - t/T)^{\frac{1}{2}} \sin \left[-\Omega T \ell n\ (1 - t/T)\right] + O(\epsilon^2) \ ,$$

where $T = L/V_0$, $\Omega^2 = \omega_{cb} V_0/r_c$, $r(0) = r_0$, $\dot{r}(0) = V_0 \alpha_0$, $\dot{z}(0) = V_0$, $\alpha_0 \ll 1$ and $(\Omega T)^{-1} \ll 1$. Using conservation of energy

$$\dot{z} = (V_0^2 - \dot{r}^2)^{\frac{1}{2}} = V_0 - \dot{r}^2/(2 V_0) + O(\epsilon^3) \quad , \tag{37}$$

The $O(\epsilon^2)$ correction to z(t) can be calculated.

Thus ion trajectories converge radially but not as quickly as the tapered channel since the perpendicular energy also increases in time at the expense of the parallel energy. From Eqs. (36) and (37) one finds that the radial envelope of the ion orbit decreases as

$$\bar{r}(r_o,\alpha_o,z) = \left(r_o^2 + \frac{V_o r_c \alpha_o^2}{\omega_{cb}}\right)^{\frac{1}{2}} (1-z/L)^{\frac{1}{2}} \quad , \tag{38}$$

and the angle with which the ion crosses the axis increases as

$$\left.\frac{dr}{dz}\right|_{r(t)=0} = \left(\alpha_o^2 + \frac{r_o^2\,\omega_{cb}}{r_c V_o \cos\alpha_o}\right)^{\frac{1}{2}} (1 - z/L)^{-\frac{1}{2}} \quad . \tag{39}$$

As the ion approaches z = L, the channel acts as a mirror and reflects the ion back toward z = 0. The approximate position of the mirror can be found by setting $dr/dz|_{r(t)=0} = \pi/2$ in Eq. (39). Because the analysis breaks down in the mirror region, the orbit equations do not describe this bounce. The analysis is not extended here to treat this region since, for reasons which follow, a target would be placed in front of the mirror point.

Since the current density scales as

$$J \sim [\bar{r}(z)]^{-2} \sim (1 - z/L)^{-1} \quad , \tag{40}$$

the current density can be considerably enhanced by radial compression of the beam. However, if radial compression is used in conjunction with axial bunching, then the spread in arrival times at the target location sets a limit on the power multiplication factor. Since radial compression produces a spread in $\dot{z}$, optimizing the power multiplication will in turn limit the degree of radial compression which should be used.

Averaging Eq. (37) over the fast oscillations, shows that the average axial velocity

$$\langle \dot{z} \rangle = V_0 \left[1 - \tfrac{1}{8} \left(\alpha_0^2 + \Omega^2 r_0^2 / V_0^2 \right) (1 - z/L)^{-1} \right] , \tag{41}$$

depends on the injection radius r_0 and injection angle α. The maximum $\langle \dot{z} \rangle$ occurs when $\alpha = r_0 = 0$ and the minimum $\langle \dot{z} \rangle$ occurs when $\alpha_o = \alpha_m$ and $r_0 = r_s$. The spread in $\langle \dot{z} \rangle$ is then just

$$\delta \langle \dot{z} \rangle = (V_0/4) \left(\alpha_m^2 + \Omega^2 r_s^2 / V_0^2 \right) (1-z/L)^{-1} , \tag{42}$$

and the resultant spread in arrival times of simultaneously injected ions in

$$\Delta t_a = (L/4V_0) \left(\alpha_m^2 + \omega_{cb} r_s^2 / V_0 r_c \right) \ell n \left(\frac{L}{L-z_t} \right) , \tag{43}$$

where z_t is the target position. If the channel were not tapered, Eq. (43) would reduce to $(\Delta t_a)_s$ given in Eq. (14). Clearly, the tapered channel can significantly increase Δt_a, which is an important consideration when axial bunching is employed along with radial compression.

Under ideal circumstances, the diode voltage can be programmed to bunch the beam at the target, the tail of the beam catching up to the front of the beam at $z=z_t$. The power multiplication factor is then expressed as

$$M = \frac{\tau_b}{\Delta t_a} \left[\frac{\bar{r}(r_s, \alpha_m, 0)}{\bar{r}(r_s, \alpha_m, z_t)} \right]^2 , \tag{44}$$

where τ_b is the beam pulse length and $\bar{r}$ is defined in Eq. (38). Here,

$\tau_b/\Delta t_a$ measures the power multiplication due to axial bunching and the expression in the square brackets measures the power multiplication due to radial compression. Since this analysis only applies for $\bar{r}(r_s, \alpha_m, z) \leq r_c\,(1-z/L)$ (i.e., all ions are confined within the channel), the most interesting case occurs when $\bar{r}(r_s, \alpha_m, z_t) = r_c(1-z_t/L)$. In this case

$$M = \frac{2m_i c^2 \tau_b\, V_o^2/eLI_o}{(1-z_t/L)\ \ell n\ \left[(1-z_t/L)^{-1}\right]} \quad . \tag{45}$$

Maximizing M with respect to z_t yields

$$M^* = \frac{8V_o \tau_b I_o^*}{LI_o} \quad , \tag{46}$$

$$Z_t^* = L\ [1-\exp\ (-\tfrac{1}{2})] \quad , \tag{47}$$

and

$$r_c^* = r_s\ \exp\ (\tfrac{1}{4})\ (1-I_o^*/I_o)^{-\frac{1}{2}} \quad , \tag{48}$$

where I_o must exceed I_o^* and

$$I_o^*(A) = 2.6 \times 10^7\ \mu\alpha_m^2\ V_o/c \quad . \tag{49}$$

Comparing this result with the power multiplication factor, M^S, obtained by using only axial bunching in a straight channel, shows that

$$M^* = 2\ [\exp(\tfrac{1}{2}) - 1]\ M^S \simeq 1.3\ M^S \quad . \tag{50}$$

Thus using radial compressions in conjunction with axial bunching can enhance the power multiplication factor by as much as 30%. Radial compression will be somewhat less effective if angular motion is present in the beam.

V. EFFECTS OF SMALL AXIAL ELECTRIC FIELDS

The axial electric field that establishes beam current neutralization by driving a return current of plasma electrons in the channel also slows down the ion beam and causes it to spread radially.[3] In order to estimate the extent of these effects, Eqs. (4) and (5) are solved with the addition of a small constant axial electric field E_z in Eq. (5). In that case

$$Z'' = R'R - \epsilon^2\delta_z \ , \tag{51}$$

where $\delta_z \equiv (\epsilon^2/r_c\omega_{cb}\, V_0 \cos\alpha_0)^{\frac{1}{2}} (E_z/B_0)$. Here a careful analysis is required since the ion kinetic energy now decreases in time.

Writing $\xi = \epsilon^2\tau$ and $\eta = (1 + \omega_1\epsilon + \omega_2\epsilon^2 + \ldots)\tau$, the time derivatives are replaced by

$$\frac{d}{d\tau} = \epsilon^2 \frac{\partial}{\partial \xi} + (1 + \omega_1\epsilon + \omega_2\epsilon^2) \frac{\partial}{\partial \eta} + \ldots \ ,$$

$$\frac{d^2}{d\tau^2} = 2\epsilon^2 \frac{\partial^2}{\partial \xi\, \partial \eta} + (1 + 2\,\omega_1\epsilon + 2\,\omega_2\epsilon^2 + \omega_1^2\,\epsilon^2) \frac{\partial^2}{\partial \eta^2} + \ldots \ ,$$

with R and Z depending on both ξ and η. Expanding Eqs. (4) and (51) and collecting terms in powers of ϵ again results in a set of equations which can be solved to any desired order in the small parameter ϵ. Here, however, the axial streaming velocity, V, gradually decreases and the radial envelope of the ion orbit, $\bar{r}$, slowly expands on the ξ time scale. The elimination of secular terms provides the set of equations which determine $V(\xi)$ and $\bar{r}(\xi)$, but the $O(\epsilon^3)$ equation of Eq. (4) is needed for completeness. The resulting spread in radius for a given ion becomes

$$\bar{r}(z) = (r_0^2 + r_c\, V_0\, \alpha_0^2/\omega_{cb})^{\frac{1}{2}} (1 - z/z_r)^{-\frac{1}{2}} \ , \tag{52}$$

where the radial expansion distance is

$$z_r = \frac{2m_i V_o^2 \cos^2 c_o}{eE_z} \qquad (53)$$

The slowing down of the streaming velocity results in a decreasing ion kinetic energy which can be expressed as

$$V^2(\xi) = V^2(0)\ (1 - z/z_r)^2 \approx V^2(0)\ (1 - 2\ z/z_r), \qquad (54)$$

where the last approximate equality applies only for $z << z_r$.

The condition for the neglect of the effects of small axial electric fields on the ion orbits is just $z_r/z_t >> 1$ or

$$eE_z z_t/m_i\ V_o^2 << 1 \qquad (55)$$

for $\alpha_m << 1$. Thus there is a lower limit set on the channel conductivity in order to prevent the axial electric field, $E_z = J_b/\sigma$, required for current neutralization, from violating the condition set in Eq. (55). Typically one would like $E_z < 1.0$ kV/cm for negligible beam energy loss.

In addition, it can be shown that when E_z satisfies Eq. (55) the spread in ion arrival times, $(\Delta t_a)_z$, at the target position is not significantly increased by the presence of E_z. In fact, in that case

$$(\Delta t_a)_z/(\Delta t_a)_s = 1 + eE_z\ z_t/m_i V_o^2 \ .$$

Thus, axial bunching is unaffected by the presence of an axial electric field if Eq. (55) is satisfied.

VI. EFFECTS OF SMALL RADIAL ELECTRIC FIELDS

The effect of a small radial electric field on the ion beam orbits can be understood by including $E_r = \bar{E}_r\, r/r_c$ in Eq. (4). In that case

$$R'' = (-Z' + \epsilon\delta_r)\, R\,, \tag{56}$$

where $\delta_r = (c^2/\omega_{cb}\, r_c\, V_o \cos\alpha_o)^{\frac{1}{2}}\ (\bar{E}_r/B_o)$. The basic effect is to weaken the restoring force in the radial equation of motion, which results in a larger radius beam. Performing the analysis of Eqs. (5) and (56) using the expansions shown in Eqs. (6), (7), and (8), the ion orbits can again be solved to any desired order in the small parameter ϵ. From this analysis, the phase mixed beam envelope is found to be

$$\bar{r}_{br} = \bar{r}_b \left(1 + \frac{r_c\, \epsilon \tan^2\alpha_m}{2\,\omega_{cb}\,\bar{r}_b^2}\ \frac{\bar{E}_r}{B_o}\right), \tag{57}$$

where the phase mixed beam envelope in the absence of E_r is defined by

$$\bar{r}_b = \left[r_s^2 + (r_c V_o \sin^2\alpha_m/\omega_{cb}\cos\alpha_m)\right]^{\frac{1}{2}}\,. \tag{58}$$

This expression is obtained from $\bar{r}$ by setting $r_o = r_s$ and $\alpha_o = \alpha_m$.

The condition from Eq. (57) for neglect of radial electric field effects on radial expansion is then

$$\bar{E}_r << \frac{2\, m_i \bar{r}_b^2\, \omega_{cb}^2}{e\, r_c \tan^2\alpha_m} \approx 1.92 \times 10^{-4}\ \left(\frac{\bar{r}_b^2\, B_o^2}{r_c \tan^2\alpha_m}\right)\ \text{Volts/cm} \tag{59}$$

where the last equality applies for proton beams with $\bar{r}_b$ (cm), r_c (cm) and B_o (gauss) measured in Gaussian units. For a 5 MeV proton beam with

$\bar{r}_b = r_c = 0.6$ cm, $\alpha_m = 0.2$ radians and $B_o = 40.0$ kG, Eq. (59) becomes $\bar{E}_r << 2 \times 10^3$ kV/cm. Typically, this condition is easily satisfied since E_r is determined only by magnetohydrodynamical effects and thermal effect.[3]

From this analysis, one can also show that axial bunching is unaffected by the presence of small radial electric fields.

The beam ion orbits given in Eqs. (9) and (10) for a straight channel or in Eqs. (35) and (36) for a tapered channel are then appropriate if the conditions on I_o, E_z and E_r set forth, respectively, in Eqs. (11), (55), and (59) are satisfied. Under these conditions the beam propagates within the channel with an envelope $\bar{r}_b$ given in Eq. (58) for a straight channel and in Eq. (38) for a tapered channel and experiences negligible radial spreading or slowing down while traveling a distance z_t, the length of the channel.

VII. PROPAGATION IN A BUMPY CHANNEL

Since the z-discharge plasma channel is formed microseconds before beam injection, the possible growth of sausage type instabilities can make the channel appear bumpy when the beam is injected. It is of value to understand how this bumpiness will affect beam propagation over distances of a few meters. Consider the situation where the channel radius varies sinusodially in z such that the magnetic field is given by

$$B_\theta = \left\{ \begin{array}{ll} \dfrac{B_o r}{r_c \left(1 - \frac{\Delta}{2} \cos \kappa z\right)^2} & , \quad r < r_c \left(1 - \frac{\Delta}{2} \cos \kappa z\right) \\ \dfrac{B_o r_c}{r} & , \quad r > r_c \left(1 - \frac{\Delta}{2} \cos \kappa z\right) \end{array} \right\} , \tag{60}$$

where $B_o = 2I_o/cr_c$, I_o is the channel current and $2\pi/\kappa$ is the wavelength of the bumps. If $\Delta << 1$, then the magnetic field inside the channel is approximately

$$B_\theta \simeq (B_o\, r/r_c)\, (1 + \Delta \cos \kappa z) \quad , \tag{61}$$

and the radial equation of motion for a beam ion which is confined within $r < r_c\,(1 - \Delta/2)$ becomes

$$\ddot{r} = - (\omega_{cb}\, \dot{z}\, r/r_c)\, (1 + \Delta \cos \kappa z). \tag{62}$$

Using Eq. (62) and the energy conservation equation, an equation for r(z) can be obtained,

$$\frac{d^2 r}{dz^2} = - \left(\frac{\omega_{cb} r}{r_c V_o}\right) \left[1 + \left(\frac{dr}{dz}\right)^2\right]^{3/2} (1 + \Delta \cos \kappa z) \quad , \tag{63}$$

where $m_i V_o^2/2$ = const is equal to the accelerating voltage. Writing Eq. (63) in a more convenient form

$$\frac{d^2R}{ds^2} = -\left[1 + \left(\frac{dR}{ds}\right)^2\right]^{3/2} R\,(\beta + \varepsilon \cos 2s) \quad , \tag{64}$$

where $R = \kappa r/2$, $s = \kappa z/2$, $\beta = 4\bar{k}^2$, $\varepsilon = \beta\Delta$, and $\bar{k}^2 = \omega_{cb}/r_c V_o$. This equation closely resembles a Mathieu equation[9] and can be solved using the method of multiple scales.[5] For $\kappa r_c/2 \sim O(\varepsilon)$ and $\varepsilon \ll 1$

$$R = \varepsilon R_1 (s_0, s_1, \ldots) + \varepsilon^2 R_2 (s_0, s_1, \ldots) + \ldots ,$$

$$\frac{d}{ds} = \frac{\partial}{\partial s_0} + \varepsilon \frac{\partial}{\partial s_1} + \varepsilon^2 \frac{\partial}{\partial s_2} + \ldots ,$$

$$\beta = \beta_0 + \varepsilon\beta_1 + \varepsilon^2\beta_2 + \ldots ,$$

where $s_m = \varepsilon^m s$. Expanding Eq. (64) and collecting terms of equal order in ε^m, one obtains

$$\varepsilon^1: \quad \frac{\partial^2 R_1}{\partial s_0^2} + \beta_0 R_1 = 0 \quad , \tag{65}$$

$$\varepsilon^2: \quad \frac{\partial^2 R_2}{\partial s_0^2} + \beta_0 R_2 = -2\frac{\partial^2 R_1}{\partial s_0 \partial s_1} - R_1 (\beta_1 + \cos 2s_0) \quad , \tag{66}$$

and higher order equations. Note that the $(dR/ds)^2$ term in Eq. (64) first appears in the $O(\varepsilon^3)$ equation. The solution of these equations are oscillatory[5,9] except near $\beta = n^2$ or $\kappa = 2\bar{k}/n$ where n is a positive integer.

Since typically $\kappa \sim r_c^{-1}$ for the sausage instability, $n = 1$ is the most important case to consider. Solving Eq. (65) with $\beta_0 = 1$ yields

$$R_1 = A(s_1) \exp(is_o) + \bar{A}(s_1) \exp(-is_0) \tag{67}$$

where $\bar{A}$ is the complex conjugate of A. Substituting this expression for R_1 into Eq. (66) and removing secular terms results in an equation for $A(s_1)$. Solving this equation one finally obtains

$$r(z) = (\tfrac{1}{2} - \beta_1)^{\frac{1}{2}} [a_1 \exp(z/\bar{z}) - a_2 \exp(-z/\bar{z})] \cos(\bar{k}z)$$
$$- (\tfrac{1}{2} + \beta_1)^{\frac{1}{2}} [a_1 \exp(z/\bar{z}) - a_2 \exp(-z/\bar{z})] \sin(\bar{k}z) \quad , \tag{68}$$

where $|\beta_1| < \frac{1}{2}$, $\bar{z} = (2/\bar{k}\Delta)(\frac{1}{4} - \beta_1^2)^{-\frac{1}{2}}$ and a_1 and a_2 are constants. For $|\beta_1| \geq \frac{1}{2}$, the solutions are oscillatory. If the initial conditions for a given ion are such that $a_1 \neq 0$, the orbit of the ion will exponentially spread in radius with an e-folding length of

$$\bar{z} \geq \bar{z}_o = \frac{4}{\Delta} \left(\frac{r_c V_o}{\omega_{cb}}\right)^{\frac{1}{2}} , \tag{69}$$

where $\bar{z}_o$ applies when $\beta_1 = 0$. In order to confine such ions over a distance z_t requires $\bar{z}_o > z_t$ or

$$\Delta < \frac{4}{z_t} \left(\frac{r_c V_o}{\omega_{cb}}\right)^{\frac{1}{2}} . \tag{70}$$

This requirement is very difficult to satisfy since the orbits exponentially expand in radius. For typical parameters, such as those used previously in Fig. 4, Eq. (70) requires that the channel radius not vary by more than 0.45%! Fortunately, the resonant region is narrow and $\kappa \sim r_c^{-1}$ in typical systems[10] is well above the resonant region.

There are two possible solutions to this resonance problem: (1) prepare the channel such that $\kappa >> 2\bar{k}$ modes will be selectively excited if the channel

becomes unstable (i.e., κ is off resonance as occurs naturally), or (2) prepare the beam such that the ions will be focused if unstable $\kappa = 2\bar{k}$ modes are excited in the channel (i.e., inject ions with $a_2 >> a_1$ for $\beta_o = 1$).

If the first method is used all the ions will have stable orbits and will remain confined. As already mentioned, this method occurs naturally since $\kappa \sim r_c^{-1} > 2\bar{k}$, however, the possibility of obtaining additional focusing using the second method warrants investigation. If the second method is chosen an ion entering the channel at r_o must have an injection angle of

$$\alpha_o = \frac{dr}{dz}\Big|_{z=0} = \left(\frac{\frac{1}{2} + \beta_1}{\frac{1}{2} - \beta_1}\right)^{\frac{1}{2}} \bar{k}\, r_o \quad , \tag{71}$$

in order to exclude unstable orbits. This condition is found by setting $a_1 = 0$ in Eq. (68) so that

$$r(z) = a_2 \exp(-z/\bar{z}) \cos(\bar{k}z + \pi/4). \tag{72}$$

Here, the ions are actually strongly focused when $z_t/\bar{z} > 1$, where z_t is the channel length.

In order to ensure that an ion remains at least on a stable trajectory requires

$$|a_2/a_1| \geq \sqrt{2} \exp(z_t/\bar{z}) \quad , \tag{73}$$

where focusing occurs whenever $|a_2/a_1|$ exceeds the value of the right hand side of Eq. (73). From this result one finds that β must be known within an accuracy given by

$$\left|\frac{\beta - \beta_o}{\beta_o}\right| \leq \frac{\sqrt{2}\Delta}{3} \exp\left(-\bar{k}L\,\Delta/4\right) , \tag{74}$$

in order to choose the proper injection conditions for focusing Eq. (71). With $\beta = 4\omega_{cb}/r_c V_o \kappa^2$ and $\Delta \ll 1$ it is presently not possible experimentally to obtain the shot to shot consistency necessary to satisfy Eq. (74).

Although the possibility of obtaining additional focusing is enticing, the prospects of using a bumpy channel to achieve this goal are not very good. Thus method (1), which avoids particle resonances by selecting $\bar{k} < \kappa/2$, appears to be the best approach to prevent beam expansion. Using $\kappa \sim r_c^{-1}$ and Eq. (11) this condition on $\bar{k}$ reduces to the following condition on α_m,

$$\alpha_m < 0.5\,(1 - r_s^2/r_c^2)^{1/2} . \tag{75}$$

Thus, for a given channel radius and beam spot size smaller injection angles are preferable in order to minimize this resonant effect. In the numerical results which follow, the worst case is considered with $\alpha = 0.2$ rad which is at the upper end of the proposed operating range of 0.1 - 0.2 rad.

To this point, the analysis has only dealt with small variations in the channel radius. When larger variations in the channel radius occur, analysis of Mathieu's equation shows that the unstable resonant region about $\beta = n^2$ broadens.[9] Since $\Delta \ll 1$ no longer holds, the previous analysis of Eq. (63) breaks down and a numerical analysis is required. The equations of motion were solved for an ion injected into a bumpy channel where the large amplitude bumps were modeled by a square waveform which replaces the sinusoidal waveform given in Eq. (60). Ions move in the magnetic field

$$B_\theta = \begin{cases} 2I_0 r/cr_c^2(z) & , \; r < r_c(z) \\ 2I_0/cr & , \; r > r_c(z) \end{cases} , \qquad (76)$$

where $r_c(z)$ is the local channel radius and I_0 is the net current. The amplitude of the bump was randomly varied in order to more closely simulate the experimental situation where the "bumpiness" is not expected to be uniform. Ions were injected into the channel in the same manner as discussed in Sec. III.

Some of the results of this work are shown in Figs. 7, 8, and 9. Figure 7 shows the percentage of beam ions which are lost from the beam channel (i.e., $|r(z_t)| > r_c$) as a function of target position for a beam injected into a bumpy channel with a distribution function at $z = 0$ given by Eq. (27). When $2\pi/\kappa = 3.77$ cm and $\Delta = \frac{1}{2}$, 53% of the beam is lost at 6.0 m downstream while 9% of the beam is lost at 6.0 m downstream for $\Delta = \frac{1}{4}$. Ions are only removed from the system if $|r(z)| > 2r_c$ at some point along the trajectory of the ion.

Figure 8 clearly shows that there are fewer ions lost as the wavelength of the bumps is decreased below about 4.0 cm. Here, $2\pi/\kappa \approx 6.9$ cm satisfies the resonant condition ($\beta = 1$) found earlier for $\alpha_m = 0.2$ rad, and also agrees well with the peak of the curve in Fig. 8. The peak of the $\alpha_m = 0.1$ rad curve also agrees well with the predicted value of $2\pi/\kappa = 13.8$ cm. The resonant wavelength ($2\pi/\kappa$) regime is considerably broadened for $\Delta = \frac{1}{2}$ compared with the very narrow resonance predicted earlier for $\Delta \ll 1$. The radial beam density profile is plotted as a function of axial position in Fig. 9 for a beam injected into a bumpy channel with $2\pi/\kappa = 3.77$ cm and $\Delta = \frac{1}{2}$. As the beam propagates downstream coherence is quickly lost due to the bumpiness

of the channel; hence, beam rippling is unimportant here. As the beam proceeds farther downstream, the beam gradually expands and the radial profile develops a broad low density tail. At 6.0 m downstream 53% of the beam ions are located at radii greater than r_c, while 20% of the ions are located at radii less than $r_s/\sqrt{10}$.

Again in order to verify that azimuthal motion does not drastically modify the results, the extreme case was considered where ions are injected into the channel with equivalent spreads in v_r and v_θ. The numerical results are shown in Fig. 10 and should be compared with the results presented in Fig. 9 where only motion in the r-z plane is considered. Since more particles are injected at larger angles to the axis when azimuthal motion is included than when only r-z motion is considered, ions are lost from the channel slightly faster. Approximately 75% of the ions are lost from the channel 6 m downstream when $\alpha_m = 0.2$ rad and $2\pi/\kappa = 3.77$ cm. As with case where only r-z motion is considered, much fewer ions are lost if α_m is reduced to 0.1 radians for $2\pi/\kappa = 3.77$ cm.

The loss rate is not significantly modified when nonuniform net current profiles are considered. If $B_\theta \sim r^2$, numerical simulations show that 60% of the ions are lost from the channel after 6 m of propagation for the same parameters as used previously in Fig. 9, where $B_\theta \sim r$ and 53% of the ions were lost.

From these results, it can be concluded that, if possible, modes with $\kappa > 2\bar{k}$ should be selectively excited if the channel is unstable to sausage instability. For example, if $\kappa \geq 8\bar{k}$, then less than 2.0% of the ions will be scattered out of the beam in the first two meters of propagation even for Δ as large as ½. The most dangerous case which must be avoided arises when

$\kappa = 2\bar{k}$. It should be pointed out again that for a typical channel, the most unstable sausage mode has $\kappa \sim r_c^{-1} \sim 2.0\ cm^{-1}$ which is off resonance even for the extreme case of a 5 MeV proton beam with $\alpha_m = 0.2$ rad ($2\bar{k} = 0.9\ cm^{-1}$). For a 5 MeV proton beam with $\alpha_m = 0.1$ rad, $\kappa \sim r_c^{-1}$ is well off resonance since in this case $2\bar{k} \sim 0.45\ cm^{-1}$.

VIII. CONCLUSIONS

The purpose of this work was to establish the groundwork for a basic understanding of intense ion beam propagation in a z-discharge plasma channel. It was implicitly assumed that the channel remains unaffected by the passage of the beam. Although there is evidence[3] that this may not be a good assumption at the tail of the beam, the analysis presented here does correctly describe the physics of the forward portion of the beam. An investigation of the physical processes which will affect beam propagation at the tail of the beam is the subject of on-going research. Effects on beam propagation due to azimuthal beam ion motion are under further investigation.

The results presented here indicate that good radial confinement of the beam during propagation in a straight channel requires that the radial and axial electric fields remain small. Equations (55) and (59) set upper limits on the allowable field strengths on E_z and E_r, respectively. If the condition on E_z in Eq. (55) is not satisfied, significant radial expansion and slowing down of the beam is expected as the beam propagates downstream. If E_r does not satisfy Eq. (59), the equilibrium beam radius is significantly increased over the beam radius in the absence of E_r. These restrictions on E_z and E_r can be easily satisfied experimentally by proper choice of channel parameters. If the conditions in Eqs. (55) and (59) are satisfied, it was also found that axial bunching is unaffected by the presence of small radial or axial electric fields.

Because of the small ion injection angles, coherent rippling of the beam could continue for distances of several meters. In the absence of other significant phase mixing mechanisms, the rippling is eventually phase

mixed out due to a dependence of the ion betatron wavelength on the ion injection angle. Analytic results show that the phase-mixing distance is given by $z_m = (4\pi/3\ \alpha_m^2)\ (r_c \bar{V}_o/\omega_{cb})^{\frac{1}{2}}$ and numerical work confirms this result. The numerical analysis also shows that the beam density on axis after phase mixing can exceed the beam density on axis at injection by about a factor of two. This corresponds to a beam radius at half maximum density after phase mixing of about $1/\sqrt{2}$ times the original beam spot size at injection.

Numerical results show that azimuthal beam motion does not modify the beam ripple wavelength or the phase-mixing distance but does somewhat reduce the final beam density on axis.

Beam propagation in a bumpy channel was also investigated in order to assess the problems involved if the beam is injected into a channel which was subject to growth of sausage type instabilities. The analysis suggests that if the channel is unstable $\kappa \geq 8\bar{k}$ modes should be selectively excited in order to avoid particle resonances which could deplete the beam by radial expansion. For a typical channel, this is accomplished with little effort since the fastest growing sausage mode satisfies $\kappa > 2\bar{k}$. Using the same resonant mechanism to help focus the beam does not seem practical since unusually fine control of the beam and channel parameters is required. Numerical work shows that azimuthal beam motion does not alter these results.

Radial compression of the beam can be achieved by injecting the beam into a tapered channel. In this case the radius of the beam converges as $(1 - z/L)^{\frac{1}{2}}$ in a channel which has a linear taper, [i.e., $r_c(z) = r_c\ (1-z/L)$]. When used in conjunction with axial bunching, radial compression can enhance the power multiplication obtained from bunching alone by as much as 30% provided the beam does not burn its own channel. Radial compression will be somewhat less effective if angular motion is present in the beam.

Future work will involve using the basic understanding developed here to build a more complete and detailed picture of beam propagation in z-discharge plasma channels.

An approximate analytic expression for $n_b(r,z)$ can be obtained for the injected distribution function given in Eq. (18), if phase mixing can be ignored. This is reasonable as long as $z \ll z_m$. In this case the ions can be propagated forward in z by using Eqs. (16) and (17) with $\omega_\beta t = \pi z/\lambda_r$. Integrating the distribution function over velocity space yields

$$n_b(r,z) = N(z) \begin{cases} [r^2 + r_1^2(z)]/r & 0 < r < r_1(z) \\ 2r_I(z) & r_1(z) \le r < r_2(z) \\ [r + r_2(z)][r_3(z) - r]/2r & r_2(z) < r < r_3(z) \end{cases}, \quad \text{(A1)}$$

for $0 \le z \le z_1 = (\lambda_r/\pi)\ \mathrm{Tan}^{-1}(\bar{\omega}_\beta r_s/2\bar{V}_o\alpha_m)$,

$$n_b(r,z) = N(z) \begin{cases} [r^2 + r_1^2(z)]/r & 0 < r < r_2(z) \\ \left([r - r_1(z)]^2 + [r_2(z) + r_1(z)]^2\right)/2r & r_2(z) < r < r_1(z) \\ [r + r_2(z)]\,[r_3(z) - r]/2r & r_1(z) < r < r_3(z) \end{cases}, \quad \text{(A2)}$$

for $z_1 \le z \le z_2 = (\lambda_r/\pi)\ \mathrm{Tan}^{-1}(\bar{\omega}_\beta r_s/\bar{V}_o\alpha_m)$, and

$$n_b(r,z) = N(z) \begin{cases} [r_1(z) + r_2(z)]^2/r & 0 < r < r_2(z) \\ \left([r - r_1(z)]^2 + [r_2(z) + r_1(z)]^2\right)/2r & r_2(z) < r < r_1(z) \\ [r + r_2(z)]\,[r_3(z) - r]/2r & r_1(z) < r < r_3(z) \end{cases}, \quad \text{(A3)}$$

for $z_2 \le z \le \lambda_r/2$. Here $r_1(z) = (\bar{V}_o\alpha_m/\bar{\omega}_\beta)\sin(\pi z/\lambda_r)$, $r_2(z) = r_s\cos(\pi z/\lambda_r) - r_1(z)$, $r_3(z) = r_s\cos(\pi z/\lambda_r) + r_1(z)$, and $N(z) = 2\bar{n}_b r_s^2/r_1(z)\,[r_3(z) + r_2(z)]^2$. For $\lambda_r/2 \le z \le \lambda_r$, $n_b(r,z) = n_b(r, \lambda_r - z)$.

An approximate expression for the phase mixed density profile ($z > z_m$) is simply obtained by averaging $n_b(r,z)$ over the ripple length, so that

$$n_b^m = \frac{1}{\lambda_r}\int_o^{\lambda_r} n_b(r,z)\,dz. \quad \text{(A4)}$$

This result is plotted in the upper right hand corner of Fig. 5.

ACKNOWLEDGEMENT

This work was supported by the U. S. Department of Energy and Sandia Laboratory Contract No. 07-9062.

1. S. A. Goldstein, D. Mosher, P. F. Ottinger, and W. W. Hsing, in Inertial Confinement Fusion (Optical society of America, San Diego, California, 1978), p. W37-1.

2. G. Cooperstein, S. A. Goldstein, D. Mosher, F. W. Oliphant, F. L. Sandel, S. J. Stephanakis and F. C. Young, in Proceedings of the 3rd International Topical Conference on High Power Electron and Ion Beam Research and Technology, (Novosibirsk, USSR, 1979); D. Mosher, G. Cooperstein, S. A. Goldstein, D. G. Colombant, P. F. Ottinger, F. L. Sandel, S. J. Stephanakis, F. C. Young, in Proceedings of the 3rd International Topical Conference on High Power Electron and Ion Beam Research and Technology, (Novosibirsk, USSR, 1979); A. T. Drobot, R. J. Barker, R. Lee, A. Sternlieb, D. Mosher and S. A. Goldstein, in Proceedings of the 3rd International Topical Conference on High Power Electron and Ion Beam Research and Technology (Novosibirsk, USSR, 1979); S. A. Goldstein, G. Cooperstein, Roswell Lee, D. Mosher and S. J. Stephanakis, Phys. Rev. Lett. 40, 1504 (1978).

3. D. Mosher, D. G. Colombant, S. A. Goldstein, and R. Lee, in IEEE Conference Record - Abstracts, 1979 IEEE International Conference on Plasma Science, Monterey, CA (IEEE, New York, 1978), p. 113; J. N. Olsen, D. J. Johnson and L. Baker, Bull. Am. Phys. Soc. 24, 978 (1979).

4. S. A. Goldstein, G. Cooperstein, R. Lee, D. Mosher, and P. F. Ottinger, in IEEE Conference Record - Abstracts, The 1978 IEEE International Conference on Plasma Science, Monterey, CA (IEEE, New York, 1978) p. 112; D. Mosher and S. A. Goldstein, Bull. Am. Phys. Soc. 23, 800 (1978).

5. A. Nayfeh, Perturbation Methods (Wiley, New York 1973), p. 228

6. D. A. Hammer and N. Rostoker, Phys. Fluids 13, 1831 (1970).

7. H. Alfven, Phys. Rev. 55, 425 (1939).

8. P. F. Ottinger, D. Mosher and S. A. Goldstein, Phys. Fluids 22, 332 (1979).

9. J. Mathews and R. L. Walker, Mathematical Methods of Physics (Benjamin, New York, 1965), p. 189.

10. D. L. Book, E. Ott, and M. Lampe, Phys. Fluids 19, 1982 (1976).

FIGURE CAPTIONS

1. Trajectories of typical ions injected into a z-discharge plasma channel from the focusing region to the left.

2. Illustration of beam rippling with a coherence length of z_m. Here the beam envelope, $r_b(z)$, is plotted as a function of axial position for the distribution function given in Eq. (18). For the proposed parameters, z_m is typically a few meters and r_s is about 0.5 cm.

3. Plot of coherence length for beam rippling as a function of maximum injection angle.

4. Illustration of beam rippling at $z < z_m$ for the distribution function given in Eq. (34) with $r_c = 0.6$ cm, $\omega_{cb} = 3.8 \times 10^8$ sec^{-1}, $V_o = 3.1 \times 10^9$ cm/sec, $r_s = 0.4$ cm, and $\alpha_m = 0.2$ rad; n_b is measured in arbitrary units.

5. Illustration of nearly complete loss of coherent beam rippling at $z > z_m = 230.6$ cm for the same beam as shown in Fig. 4.

6. Illustration of nearly complete loss of coherent beam rippling at $z \approx 50$ cm due to enhanced phase mixing caused by a nonuniform channel current profile. Here $B_\theta \sim r^2$ and all beam parameters are the same as in Fig. 4.

7. Percentage of beam ions lost vs axial position for a beam injected into a bumpy channel with $r_c = 0.6$ cm, $r_s = 0.4$ cm, $V_o = 3.1 \times 10^9$ cm/sec, $\alpha_m = 0.2$, and $I_o = 1.2 \times 10^5$ A.

8. Percentage of beam ions lost vs wavelength ($2\pi/\kappa$) of the bump for a 5 MeV proton beam injected into a bumpy channel. Here $r_c = 0.6$ cm and $r_s = 0.4$ cm for both the $\alpha_m = 0.2$ rad ($I_o = 1.2 \times 10^5$ A) and the $\alpha_m = 0.1$ rad ($I_o = 3.0 \times 10^4$ A) curves. The shaded region indicates the

proposed operating regime (r_c <0.6 cm) which could develop sausage type instabilities.

9. Plot of the beam density profile at various axial positions for a beam injected into a bumpy channel. Here, $\lambda = 2\pi r_c = 3.77$ cm, $\Delta = \frac{1}{2}$, and all other parameters are the same as in Fig. 6. n_b is measured in arbitrary units.

10. Plot of the beam density profile at various axial positions for a beam injected into a bumpy channel. Here, the ions are injected into the channel with a spread in v_θ equal to the spread in v_r and all other parameters are the same as in Fig. 9.

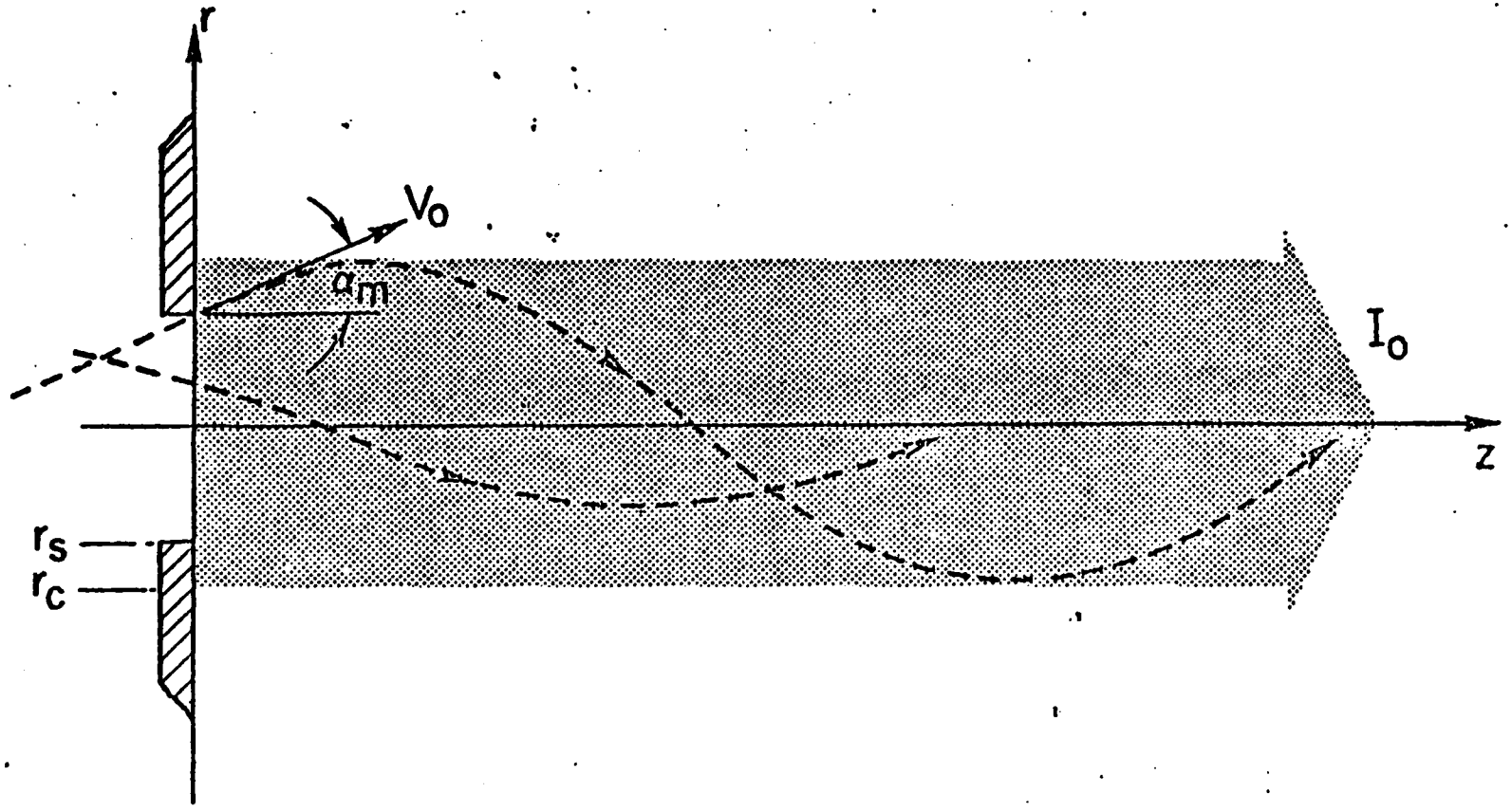

Figure 1

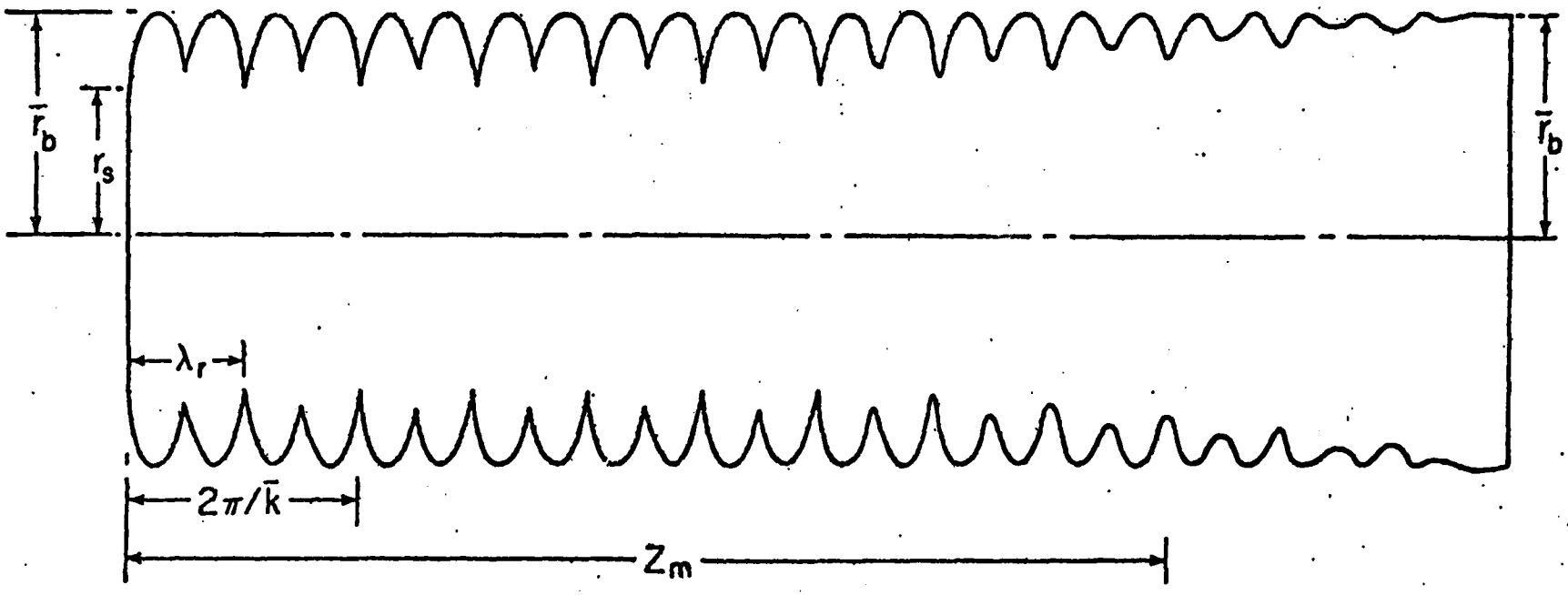

Figure 2

AD-A083 702 JAYCOR ALEXANDRIA VA F/G 20/8
AXIAL AND RADIAL COMPRESSION OF ION BEAMS.(U)
MAR 80 S A GOLDSTEIN, P F OTTINGER N00173-79-C-0420
UNCLASSIFIED JAYCOR-TPD200-80-003-FR NL

2 +2

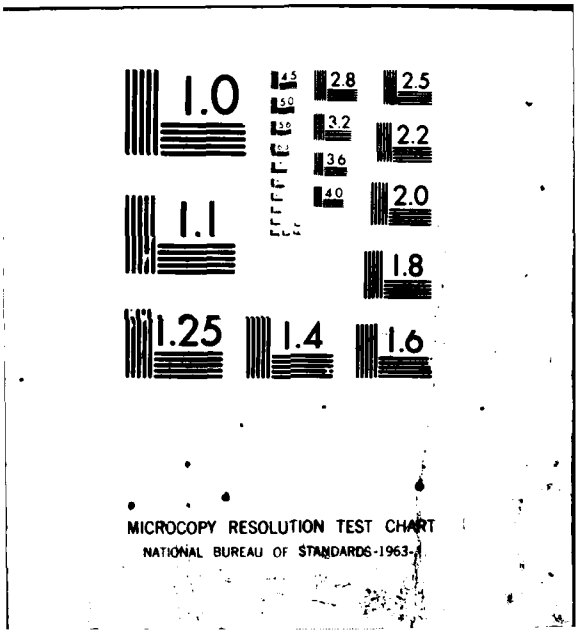
1.0
1.1
1.25
1.4
1.6
1.8
2.0
2.2
2.5
2.8
3.2
3.6
4.0
MICROCOPY RESOLUTION TEST CHART
NATIONAL BUREAU OF STANDARDS-1963-A

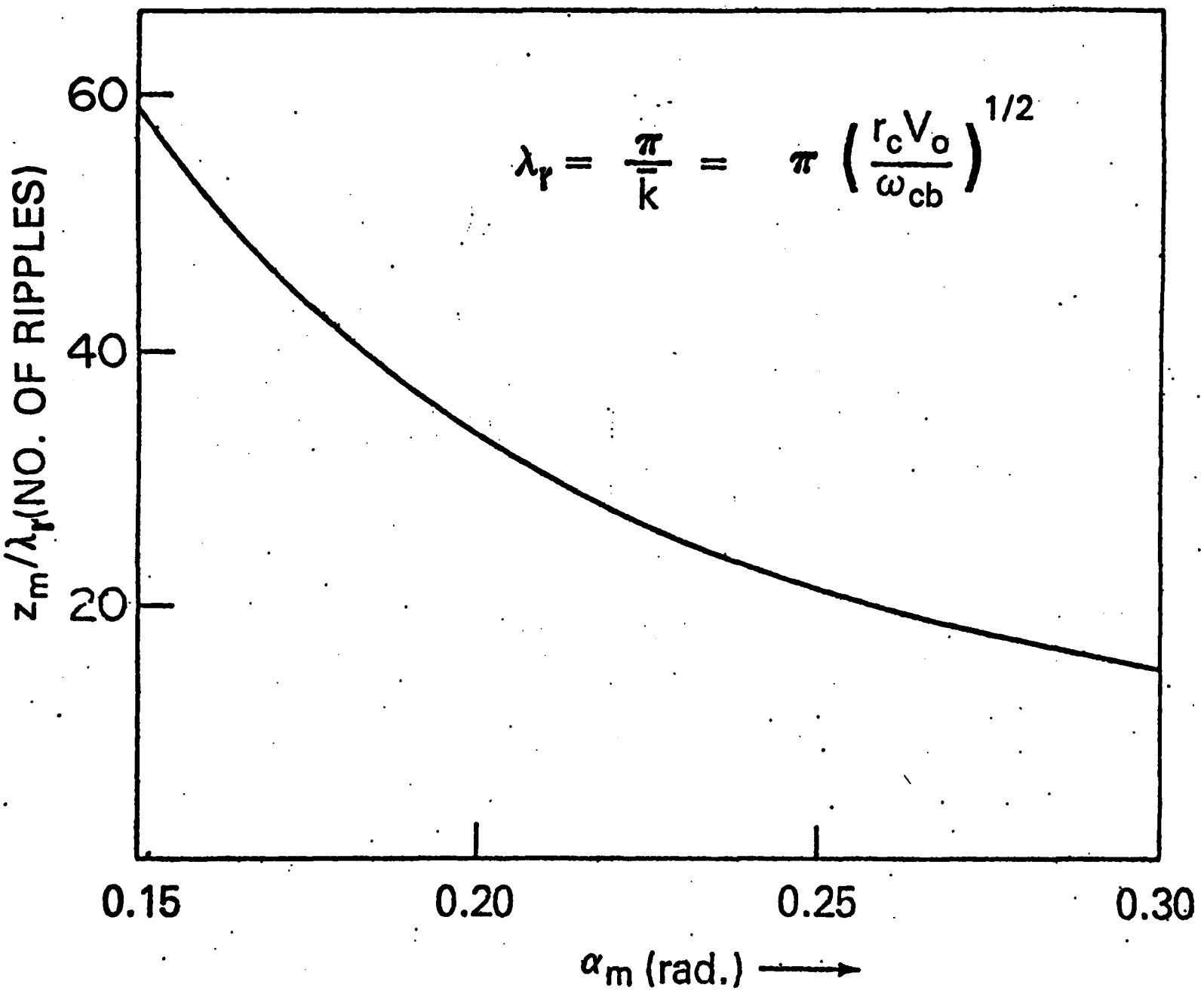
$\lambda_r = \frac{\pi}{k} = \pi \left(\frac{r_c V_o}{\omega_{cb}}\right)^{1/2}$
z_m/λ_r(NO. OF RIPPLES)
60
40
20
0.15
0.20
0.25
0.30
α_m (rad.) ⟶

Figure 3

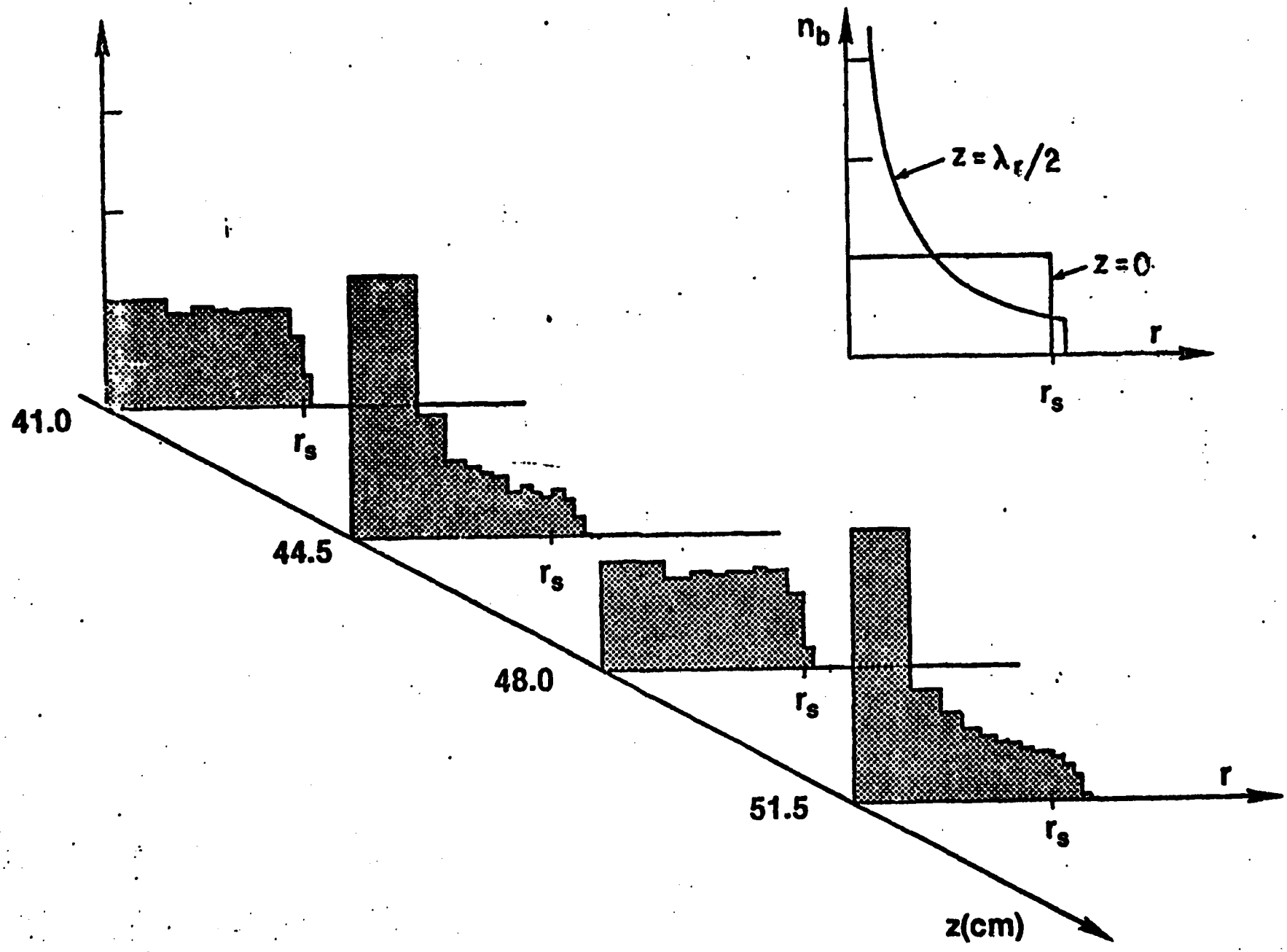

Figure 4

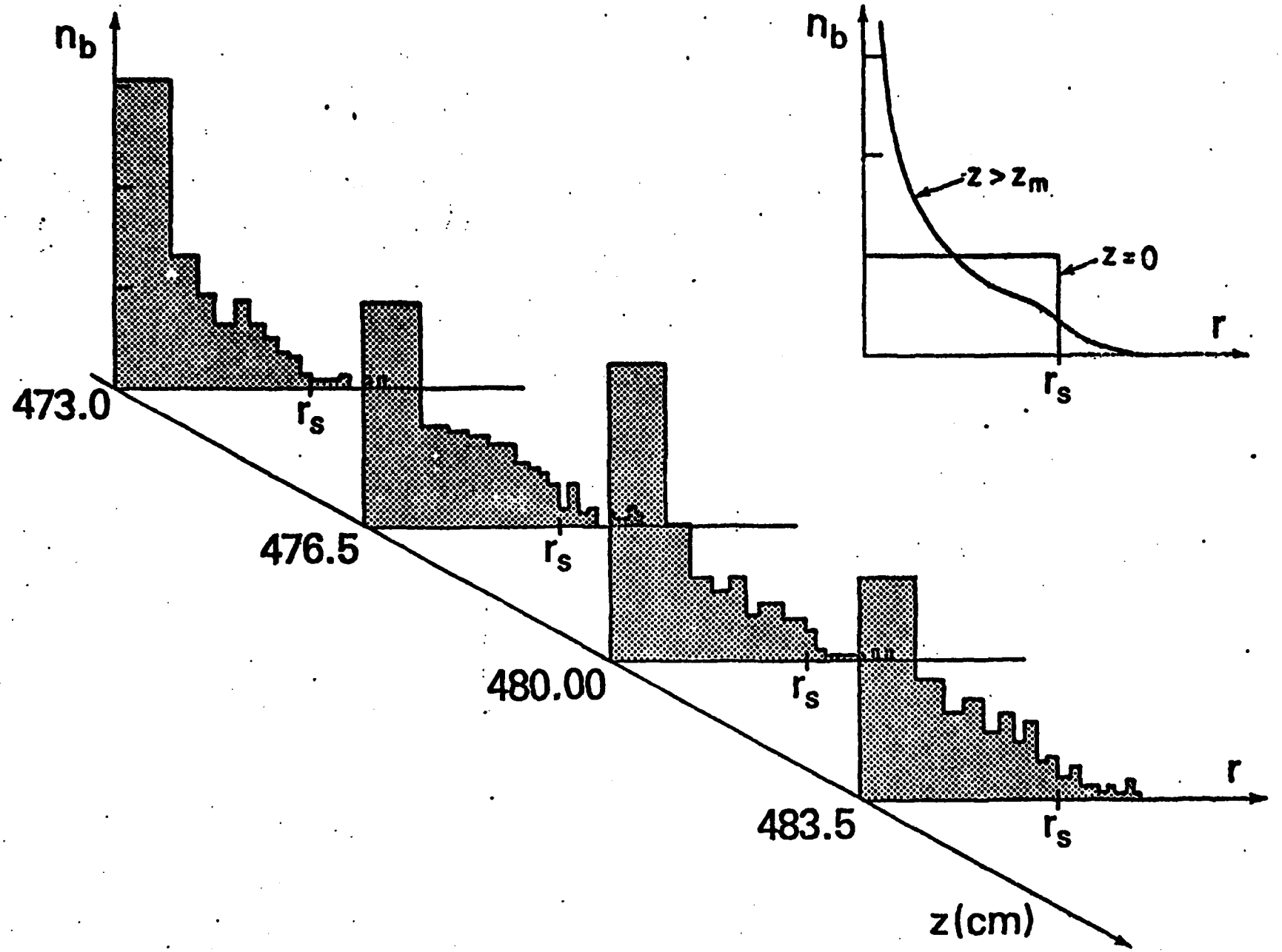

Figure 5

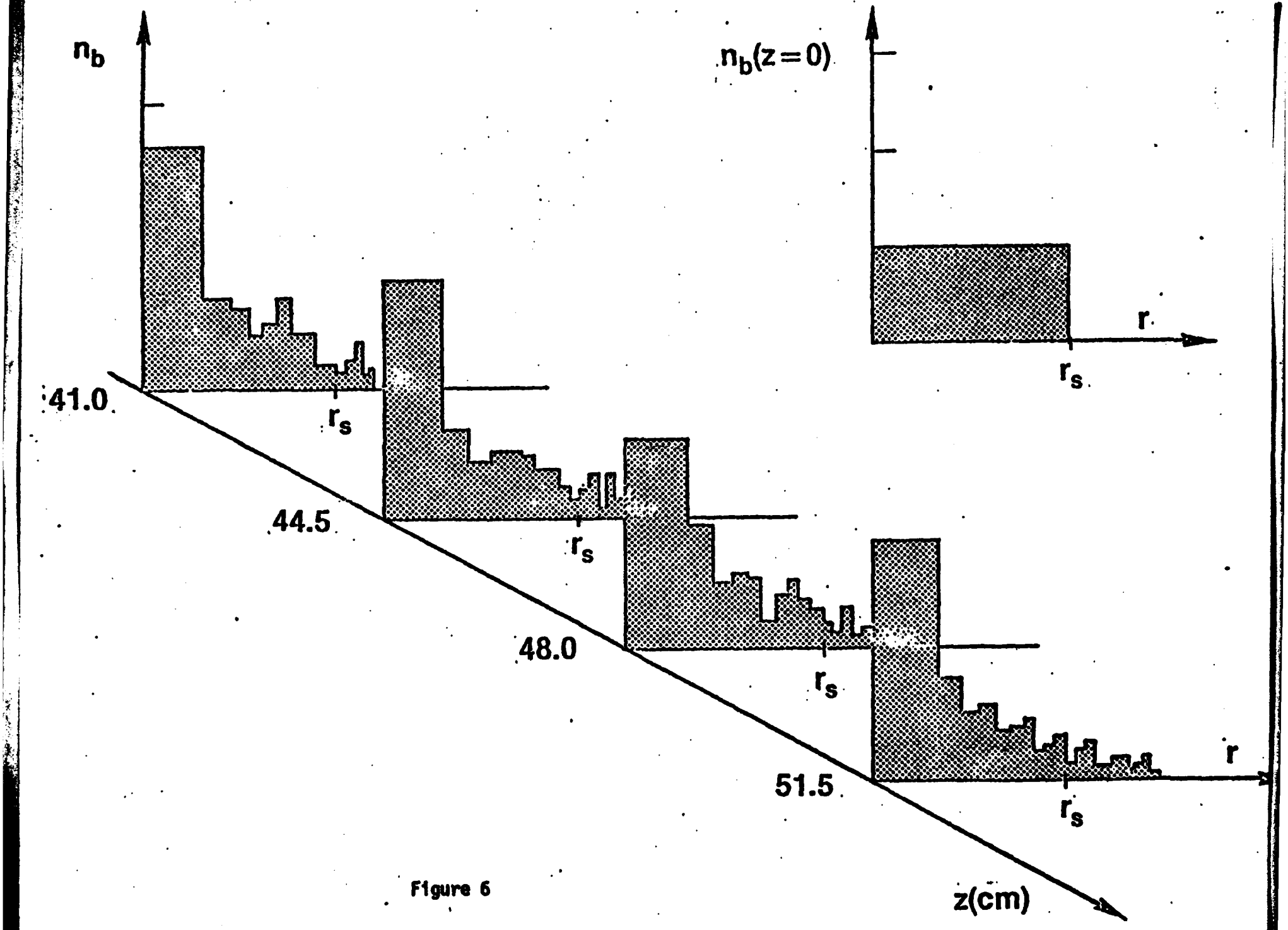

Figure 6

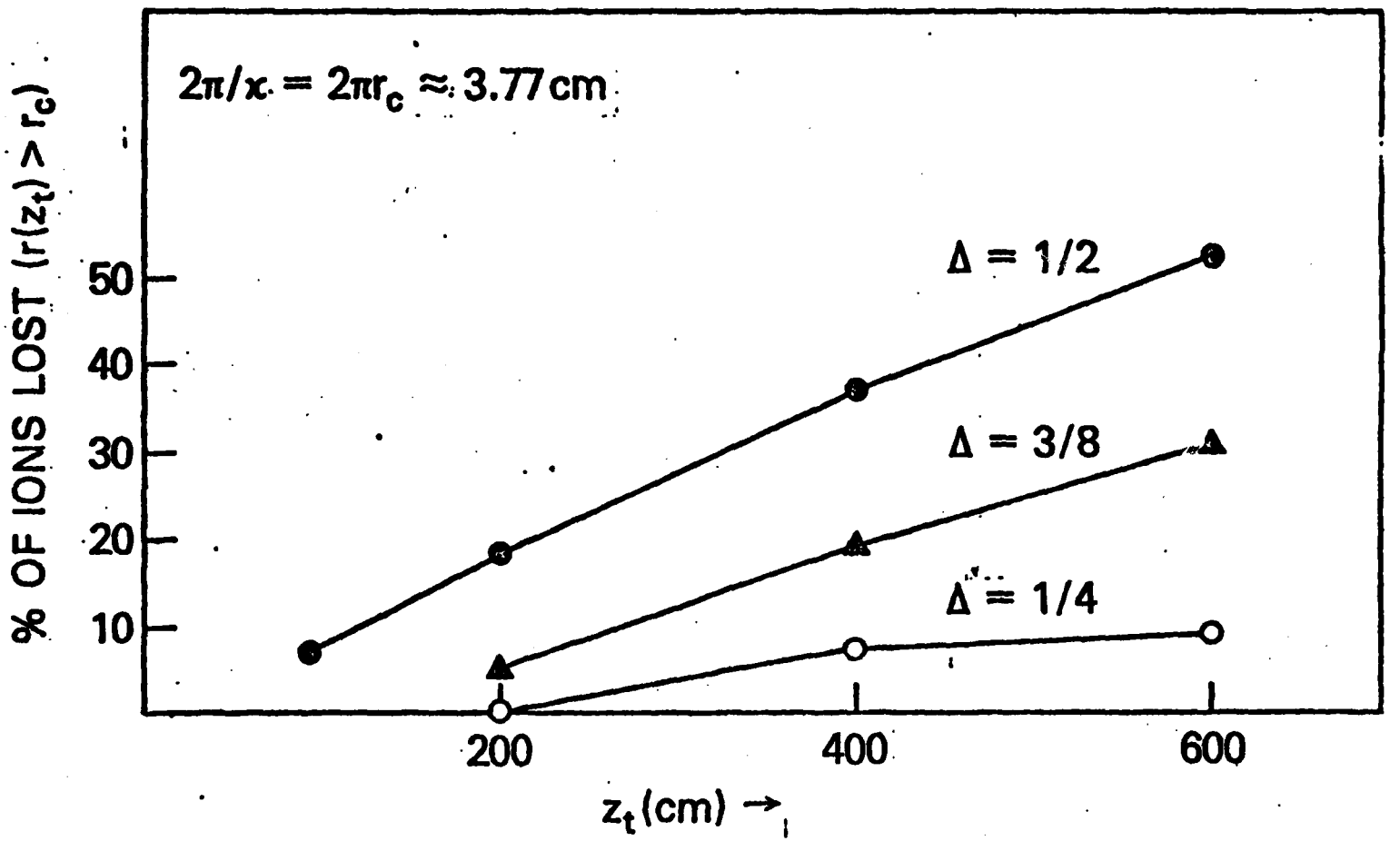
$2\pi/x = 2\pi r_c \approx 3.77\,cm$
% OF IONS LOST ($r(z_t) > r_c$)
50
40
30
20
10
$\Delta = 1/2$
$\Delta = 3/8$
$\Delta = 1/4$
200
400
600
z_t(cm) →

Figure 7

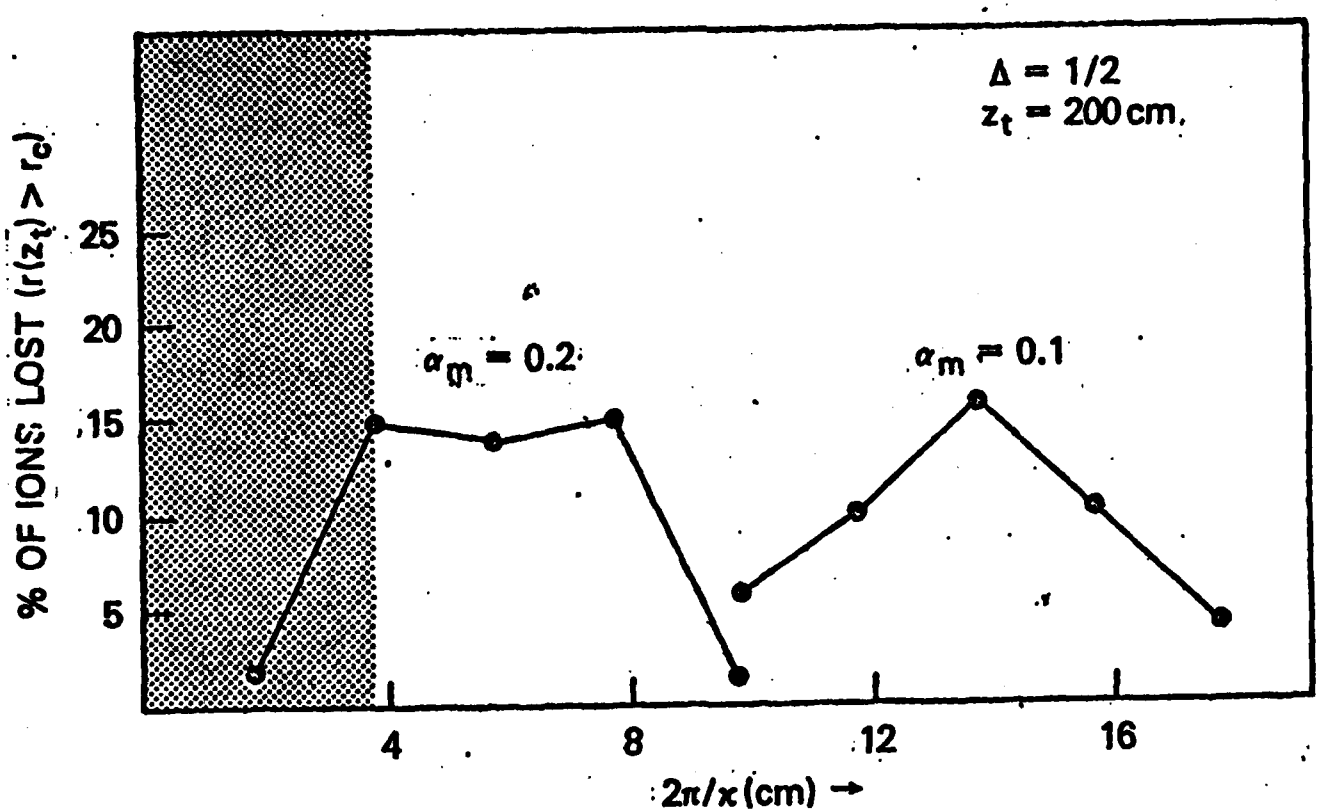
Δ = 1/2
z_t = 200 cm.
α_m = 0.2
α_m = 0.1
% OF IONS LOST ($r(z_t) > r_c$)
25
20
15
10
5
4
8
12
16
2π/x (cm) →

Figure 8

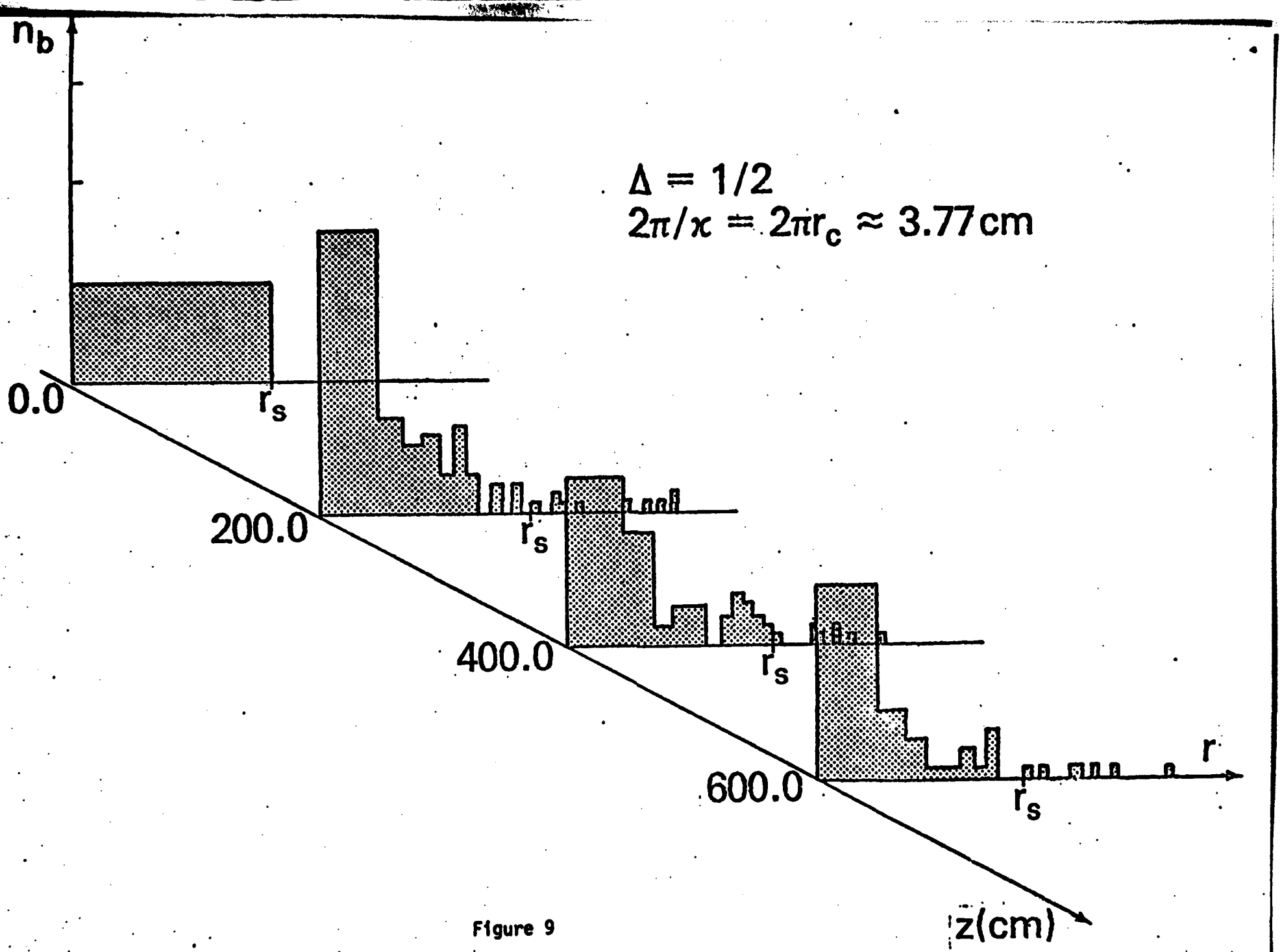
n_b
$\Delta = 1/2$
$2\pi/\varkappa = 2\pi r_c \approx 3.77\,cm$
0.0
r_s
200.0
r_s
400.0
r_s
600.0
r_s
r
z(cm)

Figure 9

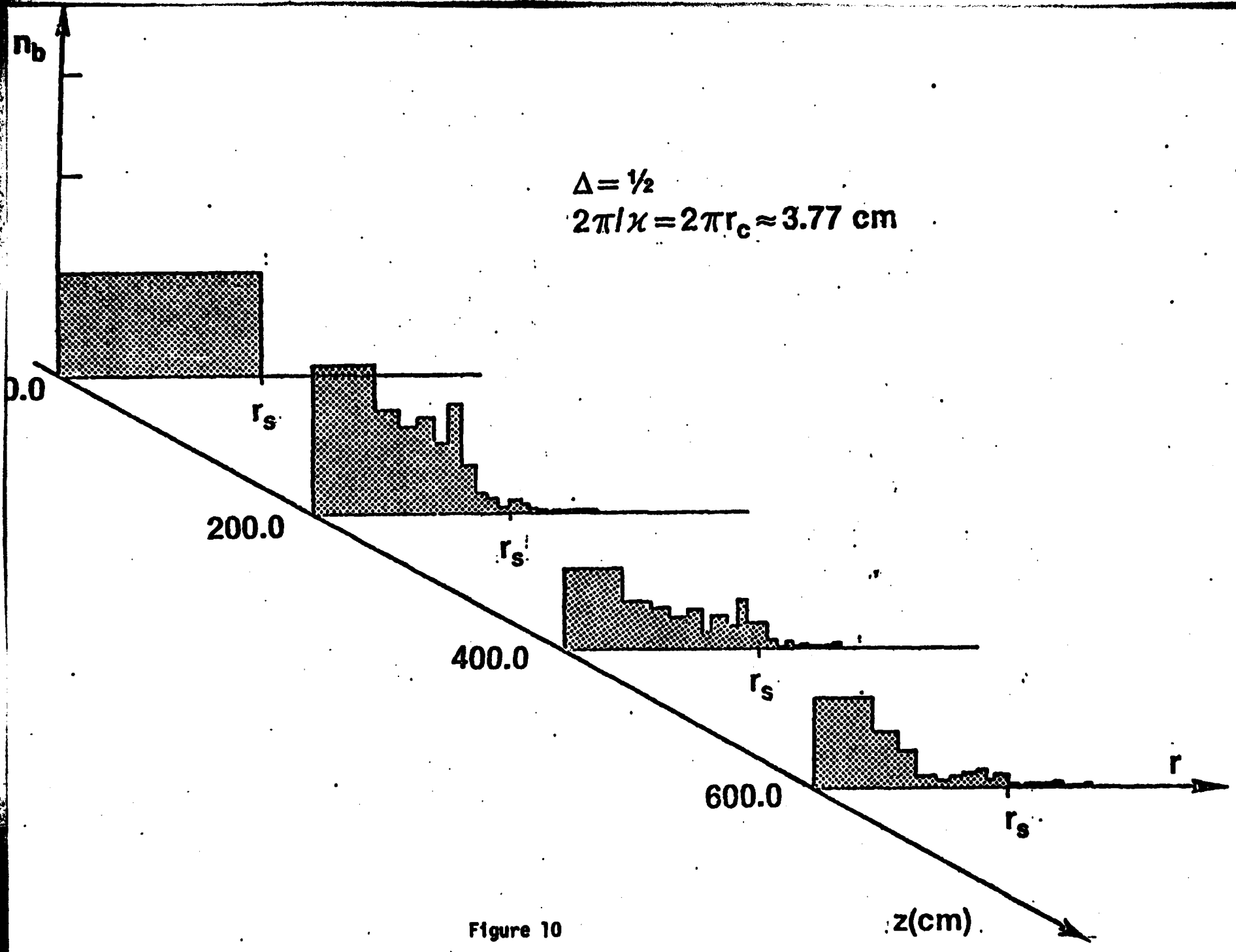
n_b
$\Delta = 1/2$
$2\pi/\varkappa = 2\pi r_c \approx 3.77$ cm
0.0
r_s
200.0
r_s
400.0
r_s
600.0
r_s
r
z(cm)

Figure 10

APPENDIX 4. Ion Orbits in a Non-Current Neutralizing Environment.

Assume an ion beam coming in paraxial under self $B_\theta(r,z)$.

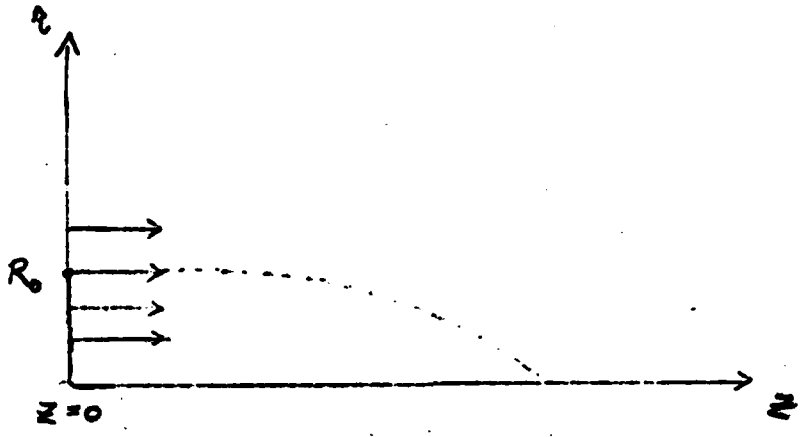

We now follow ion orbits assuming that self B_θ increases as the radius of a given ion decreases because the current envelope decreases. We also assume $\underset{\sim}{E} = 0$.

Instead of writing down all equations of motion we use energy conservation and the equation for $v_r(t)$.

$$v_r^2 + v_z^2 = v^2 \Rightarrow \frac{dr}{dt} = v_r = (-)v\left(1 - \left(\frac{v_z}{v}^2\right)\right)^{\frac{1}{2}} \tag{1}$$

$$m\frac{dz}{dt} = \frac{e}{c} v_r \times B_\theta = \frac{eB_\theta(r)}{c}\frac{dr}{dt} \Rightarrow v_z = \frac{e}{mc^2} \cdot \int_{R_o}^{r} C \cdot B_\theta(r,z)dr + v_z(z=0).$$

and since $v_z(z=0) = v$, $B_\theta = \frac{I(R_o)_{\text{Ampere}}}{5r}$, $\frac{v}{c} = 4.5\cdot10^{-2}.V_{MV}^{1/2}$

$$v_z = v\left(1 + \frac{e}{mc^2} \cdot \frac{c}{v} \cdot \int_{R_o}^{r} \frac{I}{5r}\,dr\right)$$

$$= v\left(1 + \frac{10^6 \cdot I_{MA}}{4.5\cdot10^{-2}5\cdot V_{MV}^{1/2} \cdot \frac{10^9}{300} \cdot 1} \cdot \ln(r/R_o)\right).$$

$$v_z = v\left(1 + \frac{4}{3}\frac{I_{MA}}{V_{MV}^{1/2}} \ln(r/R_o)\right) = v(1 + F(r)) \tag{2}$$

notice that $F < 0$ since $r < R_o$.

We now use Eq. (2) in Eq. (1) for $v_r(r)$.

$$v_r = (-)\, v\, (1 - (1 + F(r))^2)^{\frac{1}{2}} = (1 - 1 - 2F - F^2)^{\frac{1}{2}}$$

$$v_r = (-v)\cdot(-F^2 - 2F)^{\frac{1}{2}} = (-)v\cdot\sqrt{2}\cdot|F|^{\frac{1}{2}}\,(1 - \frac{|F|}{2})^{\frac{1}{2}}$$

$$v_r = (-)v\cdot 1.6\,\frac{I(R_o)^{\frac{1}{2}}}{V^{\frac{1}{4}}}\,\ell n^{\frac{1}{2}}\, R_o/r\,\left(1 - \frac{2}{3}\,\frac{I(R_o)}{V^{\frac{1}{2}}}\,\ell n\,\frac{R_o}{r}\right)^{\frac{1}{2}} \qquad (3)$$

It is obvious that we may integrate $\frac{dr}{dt} = v_r$ and find $r(t)$. It is, however, of interest to find the orbits directly. We now use Eqs. (2) and (3)

$$\frac{dr}{dz} = \frac{v_r}{v_z} = (-)\,\frac{1.6\, I^{\frac{1}{2}}(R_o)}{V^{\frac{1}{4}}}\,\ell n^{\frac{1}{2}}\, R_o/r\;\frac{(1 - \frac{2}{3}\,\frac{I}{V^{\frac{1}{2}}}\,\ell n\, R_o/r)^{\frac{1}{2}}}{1 - \frac{4}{3}\,\frac{I}{V^{\frac{1}{2}}}\,\ell n\, R_o/r} \qquad (4)$$

While Eq. (4) may be integrated exactly (even if R_o/r becomes big enough so that $v_z < 0$ the solution gives a correct back curved) the only problem may be particle orbit crossing and that may be cross checked after solving for $r(z,R_o)$ for different R_o and see if crossing occurs. If it does then at the crossing the whole formalism fails since the magnetic field does not follow $\frac{I(R_o)}{5r}$.

In the following we restrict ourselves to

$$\frac{4}{3}\,\frac{I}{V^{\frac{1}{2}}}\,\ell n\, R_o/r \ll 1 \qquad (5)$$

which implies for $V = 1$ MV $\quad I = 0.1$ MA that $\ell n\, R_o/r \sim 1$ to 2 is acceptable. First we use Eq. (5) in (4) and integrate the resultant equation

$$\frac{dr}{dz} = (-)\ 1.6\ \frac{I^{\frac{1}{2}}(R_o)}{V^{\frac{1}{4}}}\ \ell n^{\frac{1}{2}}\ R_o/r \qquad (6)$$

change variable to $y = \ell n\ R_o/r \Rightarrow r = R_o\ e^{-y}$

$\Rightarrow dr = (-)R_o\ e^{-y}\ dy$

$$\int_o^Y - \frac{R_o\ e^{-y}\ dy}{y^{\frac{1}{2}}} = (-)\ 1.6\ \frac{I^{\frac{1}{2}}(R_o)}{V^{\frac{1}{4}}}\ \int_o^L dz$$

In order to arrive to the same $z(=L)$ independent of the R_o for a given Y (say $Y = 1$ which gives a radius reduction by a factor e).

$$\int_o^Y \frac{e^{-y}\ dy}{y^{\frac{1}{2}}} = \frac{1.6\ I^{\frac{1}{2}}(R_o)}{R_o \cdot V^{\frac{1}{4}}}\ Z\ (Y) \qquad (7)$$

we see that the solution to Eq. (7) is a focus for all R_o if $\frac{I^{\frac{1}{2}}R_o)}{R_o} = \text{const.}$ which is $I = \text{con:}R_o^{\ 2}$ achieved only for a uniform current distribution. The distance to the focus is given by

$$Z = \frac{R_o \cdot V^{\frac{1}{4}}}{1.6 \times I^{\frac{1}{2}}(R_o)} \cdot \int_o^Y \frac{e^{-y}\ dy}{y^{\frac{1}{2}}}$$

for $Y > 1$ the integral does not grow fast and we anyway are restricted up to values of $Y \simeq 2$. We now need a tabulation of the integral as a function of Y.

Y	1	1.5	2	2.5
$\int_o^Y \frac{e^{-y}\ dy}{y^{\frac{1}{2}}}$	1.56	1.72	1.82	1.86

We use the value of $Y = 1.5$ (which gives a radius reduction by a factor of 4.5 and an area reduction of 20). The focal distance is then

$$Z = \frac{R_o \cdot V^{\frac{1}{2}}}{I^{\frac{1}{2}}(R_o)} \qquad (8)$$

for V = 0.5 MV I = 0.03 MA R_o = 1.25 cm

$$Z = 6.06 \text{ cm.}$$

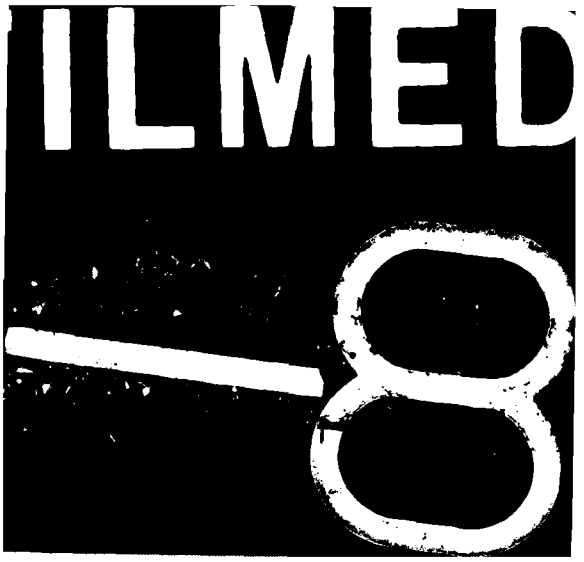
ILMED
8